DIVERGING NON-DARCY FLOW THROUGH POROUS MEDIA

Nicolino Grande

A Thesis

in

The Faculty

of

Engineering

Presented in Partial Fulfillment of the Requirements
for the degree of Master of Engineering at
Concordia University
Montreal, Quebec, Canada

August, 1981

ABSTRACT

DIVERGING NON-DARCY FLOW THROUGH POROUS MEDIA

Nicolino Grande

This is the first in a series of studies on Non-Darcy flow resistance within various configurations and under different conditions; the present work places emphasis on the effect of diverging, macroscopic streamlines.

Two permeameters were specifically designed and contructed to conduct flow/head loss experiments for parallel and radial flow.

Three homogeneous porous media were tested; spheres of 1.51 cm diameter and crushed rock in relatively uniform sizes of 2.06 cm and 3.16 cm.

The parallel flow data was utilized to establish the linear and nonlinear resistance coefficients of the Forchheimer equation; it was found that flow resistance increased with a decrease in particle size and deviation from sphericity.

Examination of the effect of diverging, macroscopic streamlines reveals an increase of approximately 5% (on the average) in the value of the nonlinear resistance term, relative to that of parallel flow, assuming the linear term to be constant for both flows. The analysis also indicates that the resistance coefficients are extremely sensitive to porosity changes.

Evaluation of the converging flow tests, carried out for the spheres only, results in a reduction of the flow resistance in the order of 20%; this confirms the trend reported in the literature.

ACKNOWLEDGEMENTS

First and foremost, I would like to thank Dr. M.S. Nasser, for his guidance and advice during my stay at Concordia. It is truly a priviledge to have worked with such an honest, sincere and dedicated person. Not only was he instrumental in the completion of this task, but I feel that he has also helped me to become a better person.

Thanks are also due to my friends Costin Antonescu, Harry Chan, Bill Feldstein, Libero Ficocelli and Wesly Fitch for their help and moral support. I would also like to thank my friend Sylvia Oh for typing the thesis.

I would also like to thank Danny Roy, in the Water Resources Lab for his aid in the construction of the permeameters.

Last, but no means least, I would like to thank my wife, Ayesha, for her patience, encouragement and love.

August 26, 1981
Montreal, Quebec

Nicolino Grande

TABLE OF CONTENTS

LIST OF FIGURES

LIST OF TABLES

CHAPTER I

INTRODUCTION

Resistance to flow through granular media is a topic of utmost importance in several fields, e.g., Petroleum Engineering, Water Resources Engineering, Soil Mechanics, etc.

Part of the Water Resources research programme at Concordia University will focus, over the next few years, on a number of studies dealing with various aspects of nonlinear flow in porous media. This work represents the initial phase toward achieving the planned research. The definition of the problem and the objectives and motivation behind the present investigation are introduced in this chapter.

The behavior of porous media flow depends on the dimension and shape of the pores, the size, shape and surface roughness of the solid particles, the flow velocity and physical characteristics of both the fluid and porous media. Basically, five flow regimes have been identified (8, 22, 23), viz; (a) Microseepage; (b) Laminar or Darcy; (c) Laminar Transitional; (d) Turbulent Transitional; (e) Turbulent.

Regimes other than Laminar are referred to as

Non-Darcy Regimes. However, only regimes c to e are relevant to the present study. A detailed discussion of the five regimes is presented in Chapter II.

Flow paths through a porous medium are tortuous and the study of flow on a microscopic scale is difficult. However, by tackling the phenomenon on a macroscopic scale, reliable results for practical application may be obtained.

Most of the previous research deals with flow resistance, assuming parallel, macroscopic streamlines. The effect of radial streamlines has received little attention. To the author's knowledge, only three studies from a converging flow field are available and one small scale study on diverging flow is reported to have given inconclusive results.

Thus, it is imperative that this first study in the series attempt to examine the effect of diverging streamlines on non-Darcy flow resistance.

A special permeameter was designed and constructed by the author to accomplish the stated goal. This permeameter can also be used to test converging flow.

Nevertheless, only when resistance in radial flow is compared to that of parallel flow can the results of the first be meaningful. Thus, it was also essential to design and construct another permeameter where the cre-

ation of parallel, macroscopic streamlines can reasonably be assumed.

An idealized medium of glass spheres of 1.51 cm diameter and crushed rock in two sizes of 2.06 cm and 3.16 cm were utilized as three homogeneous media. The characteristics of the crushed rock were determined experimentally. The findings of this study indicate that convergence would tend to enhance the hydraulic conductivity whereas divergence would impede it.

It is hoped that, upon completion of the planned research programme, more reliable estimates of the hydraulic conductivity of coarse porous media can be obtained. This will be beneficial for such problems as well flow and recharge; it can also lead to improved simulation of wave motion through rockfill embankments.

CHAPTER II

REVIEW OF THE LITERATURE

Considerable research has been conducted in the field of flow through porous media, but most of the studies have focused on flows with parallel streamlines. Radial flow has received little attention, with the emphasis being placed on converging streamlines and their effect on flow resistance. To the author's knowledge, only one study dealing with diverging, coarse porous media flow is reported in the literature, however, its findings are not conclusive.

This chapter presents the state of the art pertaining to the nature of porous media flows and the corresponding resistance equations used in their analysis.

2.1 Flow Regimes

At the outset of any discussion of porous media flow, it must be pointed out that flow through porous media may be categorized into five different regimes. Ward (22) and Wright (23) classified saturated flow into four, high velocity phases, and Kovacks (8) introduced a fifth, low velocity, regime termed microseepage. Thus, based on a modification of these studies the following are the possible

regimes:

1. Microseepage; occurs at extremely low velocities, where the molecular, rather than the viscous or inertial forces, are the dominant factors affecting the flow.

2. Darcy or laminar; in which the governing forces are the viscous forces. The flow follows definite streamlines and the hydraulic gradient is directly proportional to the first power of the velocity.

3. Laminar transitional; where both viscous and inertial forces affect the flow, but the viscous forces are predominant. The flow continues to follow definite streamlines, but some separation occurs at the downstream side of the grain walls, and the hydraulic gradient is no longer linearly proportional to the velocity.

4. Turbulent transitional; where both the inertial and viscous forces affect the flow, but the inertial forces predominate. The streamlines become unstable, and the turbulence increases. The hydraulic gradient approaches dependence on the square of the velocity.

5. Turbulent; in which the governing forces are inertial, the flow is erratic and the hydraulic gradient is proportional to the square of the velocity.

Fig. 2.1 illustrates the relationship between the hydraulic gradient, i, and the macroscopic velocity, v.

Wright (23) using a hot wire anometer found that the four different regimes could be distinguished by the Reynolds number, R_w, where R_w is defined as

$$R_w = \frac{q\, D_m}{\nu} \qquad (2.1)$$

in which

q = microscopic velocity

D_m = mean grain diameter

ν = kinematic viscosity

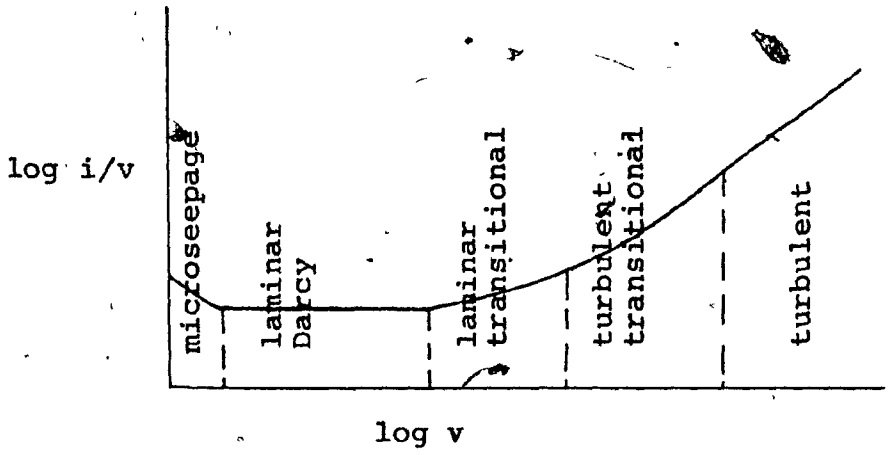

Fig. 2.1 Relationship between log v and log i/v.

Using the Reynolds number criterion, he concluded that the flow ceases to be laminar in a Reynolds number range of 1 to 5. At a value of 90 to 120 the flow starts to become turbulent transitional, and fully turbulent flow occurs at a Reynolds number of 800 or more.

2.2 The Resistance Equations

Long before the attempts, described earlier, to define the possible flow regimes, it was recognized that Darcy's law was not valid for all porous media flows. Through experiments, researchers, such as Forchheimer (4), Izbash (7), and others (3, 15, 17), suggested empirical relationships to describe non-Darcy flows. Table 2-1 lists some of the more prominent, high velocity equations and their originators.

TABLE 2-1

RESISTANCE EQUATIONS

Resistance Eq.		Proposed by	
(2.2)	$i = av + bv^2$	Forchheimer	(4)
(2.3)	$v = Mi^n$	Izbash	(7)
(2.4)	$i = av + bv^{1.5} + cv^2$	Rose	(15)
(2.5)	$v = (Bi)^{0.5}$	Escande	(3)
(2.6)	$v = (\psi/\xi)^{f-1} (\beta i)^f$	Slepicka	(17)

Note: ψ, β, ξ, a, b, B, c, f, M, n, are velocity dependent constants i is the hydraulic gradient

and 'v is the macroscopic velocity.

The two term Forchheimer equation has been shown to have a theoretical basis by Ahmed and Sunada (1). Of the five equations listed in Table 2.1, the Forchheimer equation was chosen to be used in this study.

The Escande equation can be seen to be inadequate for expressing flow resistance relationships in the transitional regimes. The Slepicka equation has a complicated form; yet it does not yield significantly more accurate results than the Forchheimer equation. The three term Rose equation was not found to yield the same accuracy as the Forchheimer equation for flows with a Reynolds number of 4000 or less; for higher values of Reynolds number, the improvement in accuracy is insignificant (11).

The majority of flows, in this study, have a Reynolds number less than 4000, therefore using the Rose equation would only increase the number of computations. Because of these reasons, the Forchheimer equation was used.

The Forchheimer equation expresses the relationship between the hydraulic gradient, i, and the macroscopic velocity, v, with two terms, the first term pertains to laminar or Darcy flow and the second term to turbulent flow. The values of the coefficients a and b, are consi-

dered constants for a particular medium and flow. Therefore, one can express flows from the laminar to the fully turbulent regimes using the Forchheimar equation.

Ward (21) attempted to quantify the a and b terms of Eq. (2.2) utilizing the characteristics of the media and fluid. Applying dimensional analysis, he deduced that a and b are given by

$$a = \frac{\mu}{k} \qquad (2.7)$$

$$b = \frac{c\ \rho}{k^{1/2}} \qquad (2.8)$$

where μ = viscosity
ρ = density of the fluid
$c = .55 \pm .024$ for all porous media

and the permeability, k, is

$$k = \frac{m^3\ \lambda^2\ D_m^2}{36\ X\ T\ (1 - m)^2\ \sigma_g^{\ln \sigma_g}} \qquad (2.9)$$

in which
m = porosity
λ = shape factor of sphericity
D_m = mean particle diameter
X = constant depending on permeameter cross-section, 1.8 for rounded and 2.0 for angular permeameters

T = tortuosity of flow path
σ_g = standard deviation of D_m

the particular shape factor, λ, is expressed as

$$\lambda = \frac{1}{m}\left(\frac{0.198}{\sigma_g} + 0.294\right) - 0.330 \qquad (2.10)$$

McCorquodale (10) modified Ward's expression of a and b and obtained:

$$a = \frac{\mu}{\rho g k} \qquad (2.11)$$

$$b = \frac{c}{g k^{1/2}} \qquad (2.12)$$

where g = acceleration due to gravity

McCorquodale et al (9) suggested two non-dimensional equations to describe steady one dimensional flow, the first equation being:

$$\frac{ig\ m\ d_r}{\upsilon\ v} = 4.6 + 0.79\ \frac{d_r\ v\ m^{1/2}}{\upsilon} \qquad (2.14)$$

in which d_r is the hydraulic radius of the pores which is used to describe the flow when the pore Reynolds number,

R_p, is less than 500. If the Reynolds number is greater than 500, they recommended that the following equation be used to describe the flow:

$$\frac{i\ g\ m\ d'_r}{\upsilon\ v} = 70.0 + 0.54\ (0.5 + 0.5\ \frac{f_e}{f_o})\ \frac{d'_r\ v\ m^{1/2}}{\upsilon} \qquad (2.14)$$

where d'_r = effective pore hydraulic radius

f_e, f_o = friction factors

The effective pore hydraulic radius is smaller than the pore hydraulic radius because of the separation of flow which occurs at the grain wells.

It should be noted that most of the flow equations are derived as if the flow occured in an infinite media without regard to boundary, but this was not the case. Dudgeon (2) and McCorquodale (10) both recognized that the wall zone in laboratory permeameters affected the flow. Allowances for this effect are applied in this study as will be described in detail at a later stage.

2.3 Radial Flow Studies

2.3.1 Converging Flow

Wright (23) was the first researcher to publish

results from a radial flow field. He plotted the Reynolds number versus the coefficient of resistance for data obtained from both parallel and converging permeameters. The following expressions were used for the Reynolds number and the resistance coefficient, respectively:

$$R_w = \frac{0.6\ v\ D_m}{\nu(1 - m)} \qquad (2.15)$$

$$\varphi = \frac{g\ i\ D_m\ m^3}{v^2\ G(1-m)\ 0.1067} \qquad (2.16)$$

where G is a function of grain shape, size distribution and surface roughness.

From his plot he found the curves, for parallel and converging flow, to be identical up to a Reynolds number of 10, beyond which convergence caused the resistance coefficient to deviate below the parallel flow value by an amount that gradually increased with increasing Reynolds number. At a Reynolds number of 100, the decrease in the resistance coefficient reached 27%.

He assumed that this decrease was due to a more uniform velocity distribution, a reduction in dead water space behind each grain and a reduction in the degree of turbulence.

McCorquodale (10) also studied the effects of

convergence, and concluded that convergence reduced resistance by 13%. He assumed that the reduction occured for reasons similar to those supposed by Wright. He also thought that the Forchheimer equation might not adequately describe converging flow.

Nasser (11) found that convergence reduced resistance by approximately 20% relative to parallel flow.

2.3.2 Diverging Flow

The sole study on diverging flow was reported by McCorquodale (10). He found that divergence caused a slight increase in resistance, relative to parallel flow, which was not statistically significant. The study was limited in scope, and the results are not conclusive.

This thesis will expand on previous work and present a comparison of parallel and diverging studies using three different types of porous media.

CHAPTER III

EXPERIMENTAL STUDY

Experimental research dealing with porous media may be separated into two distinct categories. The first is the study of the porous media itself, and the second is the study of the flow behavior through the porous media.

This chapter describes the experimental set-up designed for this study and the techniques associated with its use.

3.1 Characteristics of the Porous Media

Many properties may be adopted to classify porous media; however, the materials used in this investigation will be defined in terms of the following properties:

1. Specific Weight
2. Geometric Diameter
3. Shape Factor
4. Porosity

These properties were determined experimentally, using a fifty particle sample chosen at random from each material.

3.1.1 Specific Weight

The specific weight, γ_m, of any material can be expressed as:

$$\gamma_m = \frac{W_m}{V_m} \qquad (3.1)$$

where W_m = weight of material

V_m = volume of material

The steps performed in obtaining the specific weight of each material are:

1. The individual particles were weighed to an accuracy of $\pm$ .005 gms.
2. Each particle was carefully lowered into a calibrated cylinder filled with water to a known point of reference. The change in the water level indicated the volume of the particle.
3. Knowing both the weight, W_m, and the volume, V_m, of the material, γ_m was found by means of Eq. 3.1.

3.1.2 Geometric Mean Diameter

To obtain the geometric mean diameter, D_m, the

following equation was applied:

$$D_m = \sqrt[n]{d_{n_1} \times d_{n_2} \times d_{n_3} \ldots d_{n_n}} \qquad (3.2)$$

in which d_n was taken as the nominal diameter, that is, the equivalent diameter of a sphere with the same volume as that of the particle.

3.1.3 Shape Factor

The shape factor, λ_s, is an important term often used to express relationships in porous media flows. In this study, the shape factor is defined as

$$\lambda_s = S_s \times d_n \qquad (3.3)$$

where S_s, the specific surface is defined as the surface area, S_a, of a particle divided by its volume, V_m:

$$S_s = \frac{S_a}{V_m} \qquad (3.4)$$

For perfectly spherical particles, the surface area and volume are both functions of the diameter. Therefore; for a sphere the specific surface is simply

$$S_s = \frac{6}{d} \qquad (3.5)$$

where d = diameter of the sphere. Deviation from sphericity, however, makes determination of the surface area considerably more complicated. Several methods have been proposed for the determination of the surface area of irregular particles (11, 14, 16). All such methods may result in inaccuracies up to 25%. Since the shape factor is not directly used in this study at the present stage, this parameter was determined by visual inspection in order to give a feel of the degree of shape irregularity.

Another important property is the equivalent diameter, d_e. The equivalent diameter is defined as the diameter of a sphere having the same surface area as that of an irregular particle. It may be expressed as:

$$d_e = \left(\frac{S_a}{\Pi}\right)^{1/2} \qquad (3.6)$$

The average value of the surface area may be substituted in Eq. 3.6 to calculate the average d_e.

It should be noted that for a sphere, the terms d, d_n and d_e are all equal; therefore, the shape factor becomes 6, which is the minimum value for the shape factor since a sphere describes the minimum surface to volume ratio.

3.1.4 Porosity

It should be noted that there are two types of porosity, the drainable and the dry porosity. The drainable porosity is the ratio of the volume of the voids to the total volume in a freshly drained sample. The dry porosity is the porosity of a totally dry sample. The dry porosity, m, is the porosity that is usually used, that is:

$$m = \frac{V_v}{V_t} \quad \text{(in dry sample)} \qquad (3.7)$$

in which V_v = volume of voids

V_t = total volume

The dry in-situ porosity was determined from the permeameters as will be described in section 3.3.

3.1.5 Results

The values obtained for the specific weight, nominal and equivalent diameters, surface area, specific surface and shape factor for each of the three different porous media used in this study, are documented in Tables 3.1 to 3.3, and Table 3.4 summarizes the properties for all three materials. Also shown are the standard devi-

ations in calculating the geometric mean diameter.

3.2 Experimental Set-Up

This section is devoted to the description and method of operation of the following equipment:

1. Pumps and Valves
2. A 90° V-notch tank
3. Piezometric rack
4. Parallel flow permeameter
5. Radial flow permeameter

3.2.1 Pump and Valves

The Pump available in the Water Resources lab is a centrifugal pump, operating in a closed system. The pump has a maximum capacity of 3.0 cfs, with a maximum head of 80 feet of water. The pump delivered water directly to the permeameters which were equipped with 3" diameter Jensen valves, which controlled the incoming flow. These valves were also used at the outlets of the permeameters to control the amount of water flowing through the permeameter itself.

3.2.2 90° V-Notch Tank

A V-Notch tank was used to measure the amount of

water flowing through the permeameters. The tank is 8 feet long and has a cross-sectional area of 20 inches wide by 24 inches high. The 90° notch begins at a point 14 inches above the sill of the tank (Fig. 3.2). The procedure used to compute the flow through the tank is as follows:

1. The tank was levelled and filled with water allowing the water to flow over the V-notch.
2. The tank was then drained for two hours and the water elevation was measured. This was used as the initial water level reading, H_o.
3. While an experiment was being conducted, the water flowing though the permeameter was allowed to pass through the V-notch tank. After the flow stabilized over a period of 5 to 10 minutes, the new water level in the tank, H, was recorded.
4. The difference in water level, H, in feet was used to obtain the flow, Q, in cfs from:

$$Q = 4.2783\ C'\ (H + 0.0028)^{5/2} \qquad (3.8)$$

The coefficient of discharge, C', was found to be 0.578 for most of the discharges covered in this study.

3.2.3 The Piezometric Rack

The piezometric rack (Fig. 3.3) comprised 36 vertical tubes, whose inner diameter is 6 mm. These tubes were mounted on a board 1.5 m in height and 1.22 m wide. The board was covered with graph paper, with an accuracy of $\pm$ 1.0 mm. The tubes were connected to different points in the permeameter by means of short teflon hoses.

3.2.4 The Parallel Flow Permeameter

The parallel flow permeameter was constructed with steel and plexiglass, in three main sections (Figs. 3.4 & 3.5).

The three sections are:

1. A 3 inch inlet valve controlled the amount of water flowing through the upper section which acted as a combination stabilizer and overflow system. The water was forced to flow through a horse hair filter to eliminate entrained air, and reduce the turbulence of the incoming flow. Excess water was allowed to spill into the overflow system (Fig. 3.6).
2. A verticle plexiglass column with an inner diameter of 28 cm and a height of 122 cm formed the main control section. This section

had 12 piezometer taps drilled at 10 cm centers along one verticle side, and a stainless steel screen, which was bolted to the bottom of this section, to retain the porous media in place.

3. The lower steel section was fitted with a 3" diameter valve which controlled the amount of water flowing through the porous media. A 3" diameter flexible hose was connected to the valve and the water was fed directly into the V-notch tank, where the flow could be measured.

3.2.5 Parallel Flow Tests

The parallel flow permeameter was used to test the three porous media as follows:

1. The permeameter's central section was filled with the porous media without compaction (Note: At this time, the in-situ porosity was calculated, using the method described in Section 3.3). The permeameter was then filled with water.

2. Before connecting the piezometric tubes to the rack, they were allowed to drain into the sump to remove any trapped air.

3. The inlet valve was opened to allow water to flow through the upper section and over the overflow system.

4. The outlet valve was then opened to permit water to flow through the porous media. Both valves were adjusted to insure a saturated flow condition, and the overflow system was used to maintain a constant head (Fig. 3.6).

5. The water flowing through the overflow system was returned, by means of the sump, to the pump without being measured. The water flowing through the porous media and the outlet valve was diverted to the V-notch tank, where flow measurements could be made.

6. Having achieved equilibrium conditions, both the piezometer and V-notch readings were recorded.

7. The above procedure was repeated for different flows.

Results obtained from the parallel flow permeameter can be found in Tables 3.5 to 3.7, and Figs. 3.11 to 3.13.

3.2.6 The Radial Flow Permeameter

This permeameter was constructed in three main sections, with steel and plexiglass, much like the parallel flow permeameter (Figs. 3.7 & 3.8). The three sections may be described as follows:

1. The upper steel section has a built-in overflow system; as well as a horse-hair filter. In the converging flow experiments, this section acted as a flow stabilizer and allowed the overflow to return to the pump; thus, a constant head was maintained. The flow was forced to pass through the horse hair filter, to reduce the turbulence of the incoming water and remove any entrained air. For the diverging flow tests, the overflow system was used to collect the water flowing through the porous media, so that flow measurements could be made.
2. The central part of the device has a rectangular cross-section, with an angle of convergence or divergence of 45°. This section was constructed with 3/8" plexiglass faces bolted to 1/4" thick steel sides at 10 cm centers along the edge. The plexiglass faces were also strengthened by four steel angles bolted to

the main frame. Piezometric taps were drilled along three radial lines and the taps are spaced at 8.3 cm intervals. A stainless steel screen was fixed to the permeameter at the minimum radius of curvature, 28.7 cm. The screen was used to retain the porous media in the permeameter and to ensure radial flow exit or entrance conditions.

3. The lower section is fitted with a 3 inch diameter valve which was used to control the amount of water flowing through the porous media.

3.2.7 Diverging Flow Tests

Diverging flow tests were conducted for the three different types of porous media in the radial flow permeameter as follows:

1. The porous media was placed in the permeameter without compaction, the in-situ dry porosity was measured.
2. The permeameter was filled with water and the piezometer tubes were drained to remove any trapped air, and then connected to the piezometer board.
3. The inlet valve in the lower section was

opened to allow water to flow through the permeameter. The water flowing through the porous media was collected in the upper section, and then transported to the V-notch tank by means of the overflow and 6 inch flexible hose, respectively (Fig. 3.9).

4. Approximately 10 minutes were required to ensure steady state conditions in both the radial permeameter and the V-notch tank. The flow measurements were then taken, and the piezometric readings were recorded.

5. The procedure was then repeated to cover the selected range of discharges.

3.2.8 Converging Flow Tests

Converging flow was simulated by simply reversing the direction of flow through the radial permeameter. The tests were carried out in a manner similar to that of the diverging tests, with the following differences:

1. Water was inleted to the permeameter through the upper section, which served three functions. These functions were to maintain a constant head by means of the overflow system, to remove any entrained air and to sta-

bilize or reduce the turbulence of the incoming flow, by forcing it to flow through horse hair filters.

2. The lower section serves to control the amount of water flowing through the device, and to collect it and feed it to the V-notch tank where flow measurements were made.

3.3 In-Situ Porosity

The in-situ porosity was found for each medium in the parallel flow permeameter as well as the radial flow permeameter. The procedure was performed as follows:

1. The particles were placed in the permeameter without compaction.
2. All the piezometer taps except for the lowermost one, which was connected to the piezometer board, were sealed.
3. Water was carefully poured along one side, in order to minimize wetting of the particles, until a certain reference point was reached.
4. An amount of water of known weight and temperature was then added and the new water level recorded. The volume of water, thus

that of the voids, was determined and Eq. 3.7 was then applied to calculate the porosity.

5. Step 4 was repeated several times using the new water level as a reference each time. An average value for the porosity was then computed and used in the analysis.

3.4 Experimental Results

Table 3.5 shows the porosity values for the media in both the parallel and radial permeameters.

The data for the parallel and diverging flow experiments are documented in Tables 3.6 to 3.11. Figs. 3.11 to 3.16 illustrate graphically the relationship between the piezometric head, Φ, versus location for all the cases tested.

The data from the converging flow tests conducted only for the spheres, can be found in Table 3.12 and Fig. 3.17.

CHAPTER IV

ANALYSIS OF RESULTS

This chapter presents an evaluation of the results obtained from the experimental study. A comparison of the three types of flows will be made for the spheres; the results obtained from the diverging flow experiments for the two rock sizes will be compared to the results obtained from the parallel flow experiments.

4.1 Parallel Flow

The Forchheimer equation (Eq. 2.2) may be linearized in the form:

$$\frac{i}{v} = a + bv \qquad (4.1)$$

Utilizing the parallel flow data, and the method of least squares, the values of a and b were determined, based on a best fit line.

Figs. 4.3 to 4.5 display the $\frac{i}{v}$ versus v plots for the three porous media used in this study. Also shown is the correlation coefficient, C_c, which is used to measure the goodness of the fit.

The Reynolds number, R_m, was calculated for the discharges tested, by means of the following equation:

$$R_m = \frac{v\ D_m}{\nu\ m} \qquad (4.2)$$

where v = macroscopic velocity

D_m = nominal diameter of particles

m = porosity

ν = kinematic viscosity

The values of the Reynolds number covered in the parallel flow experiments ranged from 900 to 10,000.

4.2 Radial Flow

Based on earlier studies, reviewed in section 2.3, it was deduced that radial flow would tend to either increase or inhibit turbulence. Thus, it may be assumed that converging or diverging macroscopic streamlines would mainly affect the inertial term, b, of the Forchheimer equation. Therefore, by treating the Darcy term, a, as a constant in both parallel and radial flow, an evaluation of the b term can be made.

Invoking this assumption, Nasser(11) developed the following expression to deduce the value of b in converging flow, from a known value of a for parallel

parallel flow.

$$b_c = \frac{a_c \ln\left(\frac{r_{c_n}}{r_{c_{n+1}}}\right) - \frac{1}{C}\left(\Phi_n - \Phi_{n+1}\right)}{C\left(\frac{1}{r_{c_n}} - \frac{1}{r_{c_{n+1}}}\right)} \qquad (4.3)$$

where Φ = the piezometric head

r_c = radius of convergence

a_c, b_c = coefficients for converging flow

and C is:

$$C = \frac{Q}{\theta w} \qquad (4.4)$$

where Q = the flow in lps

θ = the angle of convergence

w = width of the permeameter

An expression based on the data of McCorquodale (10) and Nasser(11) was deduced to compute the difference in the value of b between the parallel and converging flow, viz:

$$b_c = b_p \left(1.0 - 0.13\, e^{\left(\frac{r_c}{100\, D_m}\right)}\right) \qquad (4.5)$$

where b_p is the adjusted value of b for parallel flow and r_c is the average radius of convergence of the permeameter.

Following a procedure similar to that of Nassar's, an expression for b for diverging flow was derived. — Note: that in the derivation to follow, the subscript d refers to the value of the terms in the diverging flow field.

The Forchheimer equation may be written in the form:

$$-\frac{d\,\Phi}{d\,r_d} = a_d\,v_r + b_d\,v_r^2 \qquad (4.6)$$

The hydraulic gradient, $\frac{d\,\Phi}{d\,r_d}$, is negative since it decreases in the direction of the flow, as can be seen from Fig. 4.1(b). By rearranging Eq. 4.6 into the form:

$$b_d\,v_r^2 + a_d\,v_r + \frac{d\Phi}{dr_d} = 0 \qquad (4.7)$$

and solving for v_r leads to:

$$v_r = \frac{-a_d \pm \sqrt{a_d^2 - 4\,b_d\,\frac{d\Phi}{dr_d}}}{2\,b_d} \qquad (4.8)$$

Squaring and rearranging Eq. 4.8 yields:

$$b_d \, D \, \frac{dr}{r_d^2} + a_d \frac{dr}{r_d} = - \frac{1}{C} \, d\Phi \qquad (4.9)$$

By taking: $V_r = \frac{C}{r_d}$; where $C = \frac{Q}{\theta w}$

in which Φ is the angle of divergence.

Integrating both sides of the equation from (Φ_n, r_{d_n}) to $(\Phi_{n+1}, r_{d_{n+1}})$ gives:

$$b_d = \frac{\frac{1}{C} (\Phi_n - \Phi_{n+1}) + a_d \ln \left(\frac{r_{d_n}}{r_{d_{n+1}}}\right)}{C \left(\frac{1}{r_{d_n}} - \frac{1}{r_{d_{n+1}}}\right)} \qquad (4.10)$$

where the subscript d represents diverging flow.

4.3 Effect of Porosity and Wall Zone

In order to furnish a consistent basis for a meaningful comparison of parallel and radial flow, adjustments for the differences in porosity and wall effects between the two permeameters were made. The parallel flow results were corrected to reflect the same conditions as those which existed in the radial flow permeameter.

4.3.1 Porosity Correction

Because of the porosity differences between the

two permeameters, a porosity correction must be applied. Using the expressions for a and b from Eqs. 2.7 and 2.8, with the value of K replaced by Eq. 2.9, the porosity correction, C_m, is deduced as follows:

$$C_m = \frac{\dfrac{m_p^3}{(1 - m_p)^2}}{\dfrac{m_r^3}{(1 - m_r)^2}} \qquad (4.11)$$

where the subscripts r and p refer, to the radial and parallel permeameters respectively.

The correction is applied to a and b as follows:

$$a' = a \cdot c_m \qquad (4.12)$$

$$b' = b \cdot (C_m)^{0.5} \qquad (4.13)$$

where a' and b' are the porosity corrected values.

4.3.2 Wall Correction

Dudgeon (2) suggested that the velocity distribution near the wall of the permeameter is influenced by the change in porosity due to the presence of the wall. He found its effect to be significant to a distance of half a particle diameter from the wall (Figure 4.1).

McCorquodale (10), modifying Dudgeon's expression for the wall effect correction obtained Eq. (4.14).

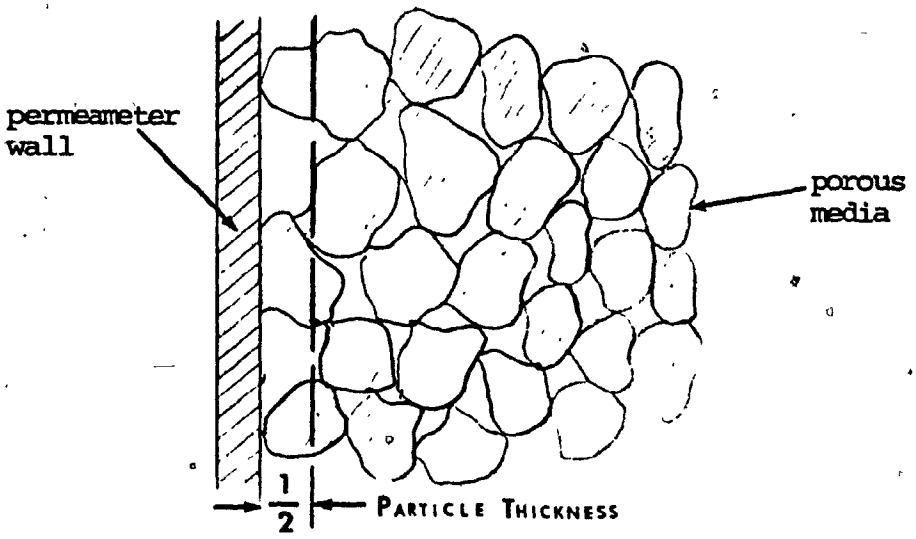

Figure 4.1 Effect of the Wall

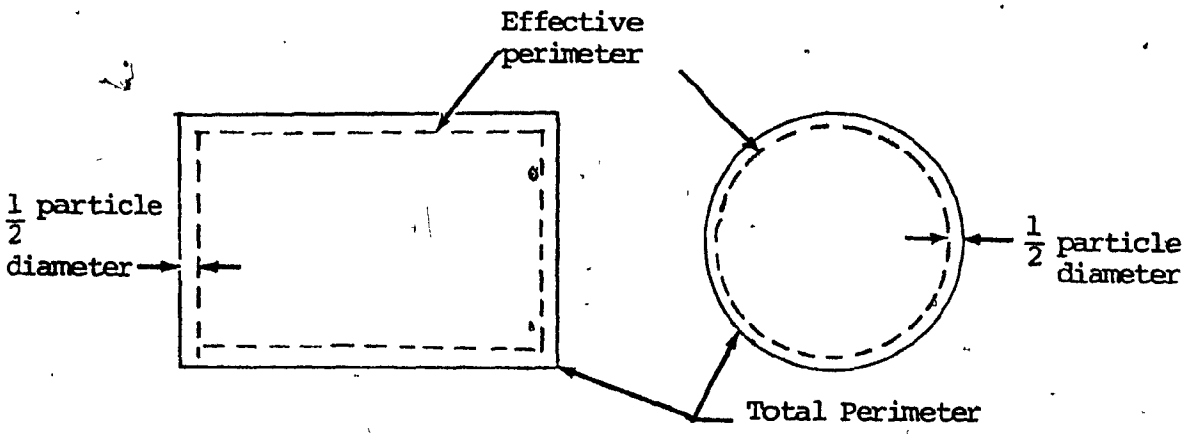

Figure 4.2 Effective Perimeter for
(a) Circular and
(b) Rectangular Permeameter.

$$W_c = [\ 1 + X_p \frac{L_e}{L_t} \frac{D_m}{A}\ ]^{-1} \qquad (4.14)$$

where W_c = wall effect correction

L_e = effective perimeter, which is is taken to be the perimeter at at a distance of half a particle diameter from the wall (Fig. 4.3)

L_t = total perimeter

A = cross-sectional area of the permeameter. For the radial permeameter, this was taken to be the average x-sectional area.

X_p = A constant to account for permeameter cross-sectional shape.
1.8 for circular permeameters
2.0 for rectangular permeameters

Dudgeon (2) noticed that the effect of the wall was almost independent of the flow rate, for any medium. Therefore, the wall correction, C_w, may be applied directly to a and b instead of v, in the following manner:

$$a'' = a \cdot C_w \tag{4.15}$$

$$b'' = b \cdot (C_w)^2 \tag{4.16}$$

where a" and b" are the parallel flow values corrected for wall effect. The wall effect correction, C_w, is given by:

$$C_w = \frac{W_{c_r}}{W_{c_p}} \tag{4.17}$$

Combining the corrections for both porosity and wall effect yields:

$$a_p = a \cdot C_m \cdot C_w \tag{4.18}$$

$$b_p = b \cdot (C_m)^{0.5} \cdot (C_w)^2 \tag{4.19}$$

Where a_p and b_p are the final corrected values of both constants. The corrections for porosity and wall effect can be found in Tabel 4.3 and the corrected values

of a and b are listed in Table 4.4.

4.4 Evaluation of the Radial Flow Results

The series of converging flow tests, conducted only for the idealized medium of spheres, was intended to assess the reliability of the performance of the radial flow permeameter. This was accomplished by comparing the results to published data on converging flow.

The converging flow data were analyzed, by means of Eq. 4.3, in pairs of r_c and Φ . Thus, for each data set, the a_c value adjusted for porosity and wall effect was inserted in the equation and the corresponding b_c was deduced. The wall correction was applied for each individual piezometer reading from the radial permeameter according to the cross sectional area where the piezometer was located.

An average value for b_c was then calculated for each discharge and compared to the average value of the adjusted parallel flow b's. Finally, the average b_c for the spheres based on all the discharges tested was compared to the corresponding average b_p .

The average b_c for the spheres was found to be 20% less than the parallel b value. This is in conformity with the values reported by Wright (23), McCorquodale (10) and Nasser (11). Further, an estimate of b_c for the spheres was obtained by Eq. 4.5.; this gave a b_c value

22% less than parallel flow; this enhances the confidence in the validity of Eq. 4.5. Hence, the values of b_c for the 2.06 cm rock and 3.16 cm rock were found by Eq. 4.5 to be, respectively, 19% and 16% lower than the appropriate parallel flow values.

Analysis of the diverging flow data for the flow medium by means of Eq. 4.10, was performed in a similar manner to that described for the application of Eq. 4.3. An increase in the b_d value of approximately 5%, on the average, over that of parallel flow was detected in each case.

Figs. 4.6 to 4.8 display scatter plots for the b_d values as compared to the parallel flow b . The b_c value, calculated by Eq. 4.5, can also be found in Table 4.4.

Fig. 4.9 illustrates the scatter in the b_c values for the spheres.

Table 4.5 summarizes and compares the results of all the a and b values obtained for the three types of flow.

4.5 Discussion

4.5.1 Parallel Flow Friction Curves

The friction curves obtained from the parallel flow data gave excellent correlations for all the porous media tested. The values of the resistance coefficients

a and b decrease with the increase in particle size. This is conceivable as the smaller the grain size , the larger the surface area exposed and thus the higher the resistance offered by the medium to the flow.

4.5.2 Significance Of The Diverging Flow Effect

The increase in resistance induced by diverging streamlines would tend to inhibit the hydraulic conductivity in non-Darcy flow;the 5% increase was consistent in all cases tested. Yet, it is the author's conviction that extensive investigations are still required before that increase can reliably be quantified.

The estimation of the resistance coefficients a and b are extremely sensitive to porosity changes. However, porosity measurements are difficult to obtain with precision. This was particularly critical in analyzing diverging flow .

The diverging flow tests were conducted by feeding the flow from the bottom upward in order to induce full flow conditions, thereby ensuring divergence of the macroscopic streamlines. Consequently, an uplift type phenomenom was noticed to cause a slight expansion of the medium and rearrangement of the particles during the experiments. As a result, the actual porosity value

during the tests was higher than that considered in the analysis. It should be noted that a small increase in porosity of 1% caused the value of b_d to increase to 9%.

Note, the kinectic energy term was incorporated in the Φ term in Eqs. 4.3 and 4.10 based on the true velocity value. Nevertheless, the effect of the velocity head was not pronounced.

Figs. 4.6 to 4.9 exhibit large scatter; however , the analysis indicates that the average value of b_d does not vary significantly from one flow to another. This further suggests that the effect of Reynolds number on this apparent diverging flow effect, and for that matter converging flow also, is minimal.

It is emphasized that many efforts have been made by researchers to establish an upper limit for the application of Darcy's law. The attempts centered around representing this upper limit by a critical Reynolds number, and many definitions of the characteristic length in the expression were suggested. The proposed values ranged between 0.1 and 75, a discrepancy which is beyond coincidence.

As no turbulence measurements were associated with the flow tests conducted in this study; the author could not determine when turbulence started. However, the range of Reynolds number covered by the exper-

iments ensures the departure from Darcy's law.

4.5.3 Experimental Errors

The experimental errors encountered in the study may be summarized as follows:

1) Flow measurement errors using the v-notch tank, were estimated to be in the order of $\pm$ 1%.

2) The piezometer board could only be read to an accuracy of $\pm$ 0.05 cm.

3) The readings were taken from piezometers tapped into the side of the permeameter. Therefore, any irregularity of the pore space caused by the presence of the wall would affect the pressure readings.

4) The error in reading the porosity could be attributed to two main reasons, the first being the retention of water by the upper pores, and the second the error inherent in the piezometer board readings.

5) An error in estimating the physical characteristics of the media could result, because of the weight which could only be measured to an accuracy of $\pm$ 0.005 gms, and the error in measuring the volume, $\pm$ 0.05 cm^3 and $\pm$ 0.5 cm^3 for the small and large particles respectively.

CHAPTER V

CONCLUSIONS AND RECOMMENDATIONS

5.1 Conclusions

Based on this study, the following conclusions are made:

1) Flow resistance in parallel non-Darcy flow increases with a decrease in particle size.

2) Converging streamlines cause the nonlinear resistance term of the Forchheimer equation to decrease by an amount of approximately 20% relative to parallel flow, provided the linear term is treated as a constant for both flows. This confirms the trend reported in the literature.

3) Divergence of streamlines was shown to increase the non-Darcy resistance coefficient by approximately 5% over that of parallel flow.

4) The variation in the values of the Darcy and non-Darcy resistance coefficients are extremely sensitive to porosity changes.

5.2 Recommendations For Future Research

The two permeameters introduced in this work were designed for long term utilization, in a number of studies, as explained earlier.

Future research should cover wider range of particle shapes and sizes and different ranges of Reynolds

Number.

A more thorough definition of flow regimes is needed; this will certainly represent an important contribution to research in the field of porous media flow.

The improvement in hydraulic conductivity caused by converging streamlines seems to be much more pronounced than the apparent opposite effect induced by diverging streamlines. Therefore, examination of diverging flow should proceed to attempt to single out the effect of divergence. This will require more care in making accurate porosity measurements and experimenting with a variety of angles of divergence.

APPENDIX A

FIGURES

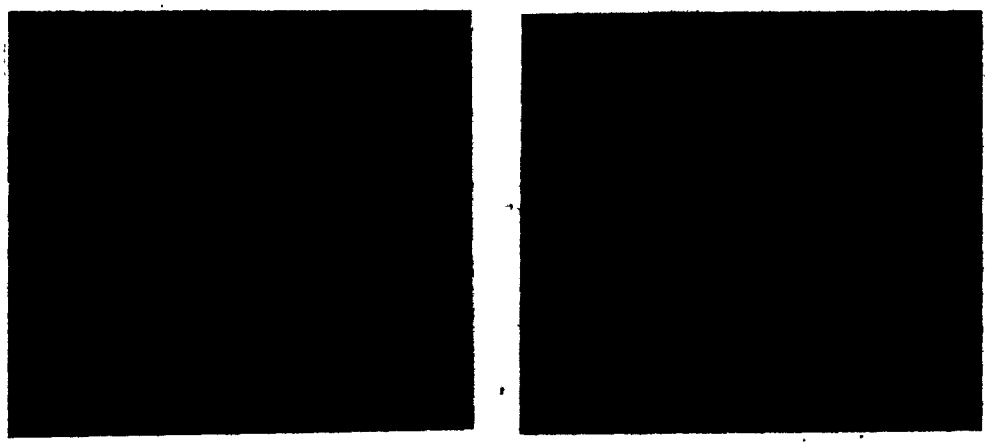

(a) Small Rocks (b) Large Rocks

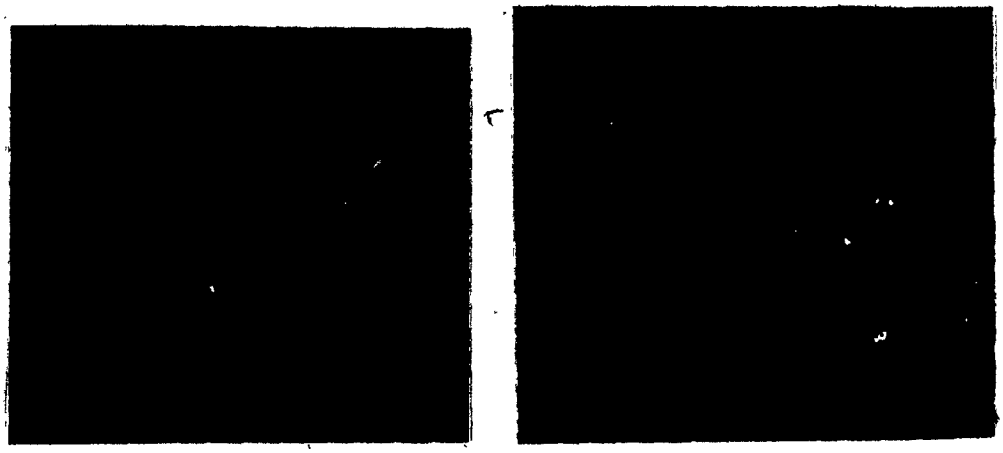

(c) Spheres (d) Comparing the Three

FIGURE 3.1 Comparison of the Three Porous Media

COLOURED PICTURE

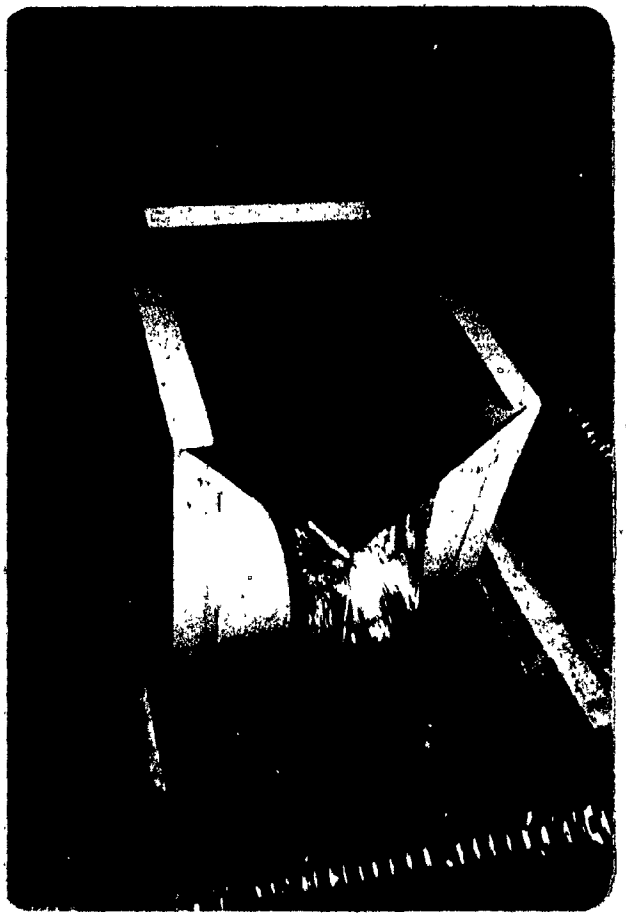

FIGURE 3.2 90° V-Notch Tank

COLOURED PICTURE

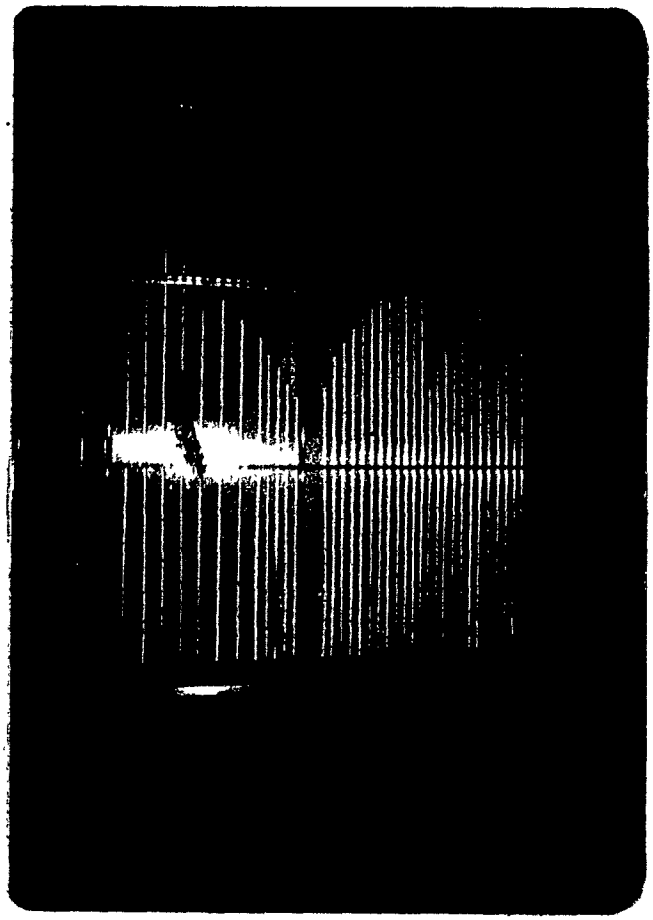

FIGURE 3.3 Piezometer Rack

COLOURED PICTURE

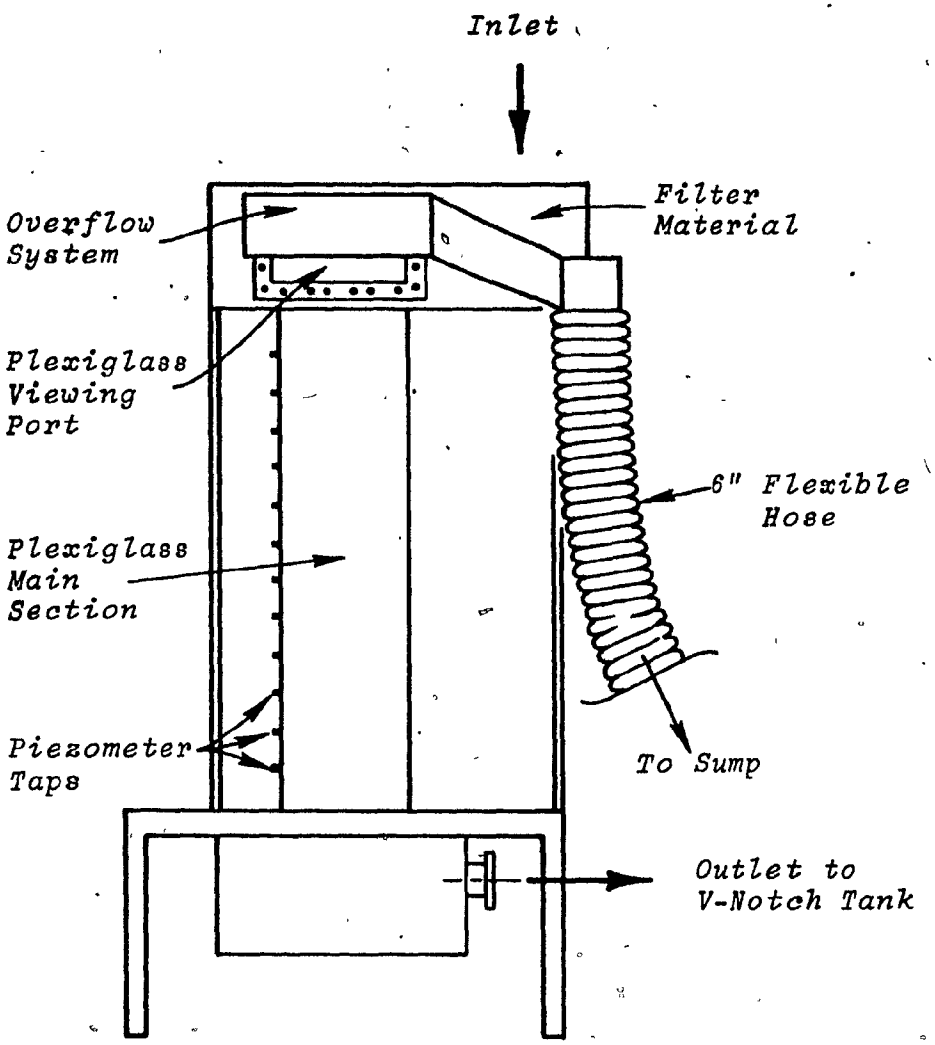

Front View

FIGURE 3.4 Schematic Diagram of the Parallel Flow Permeameter

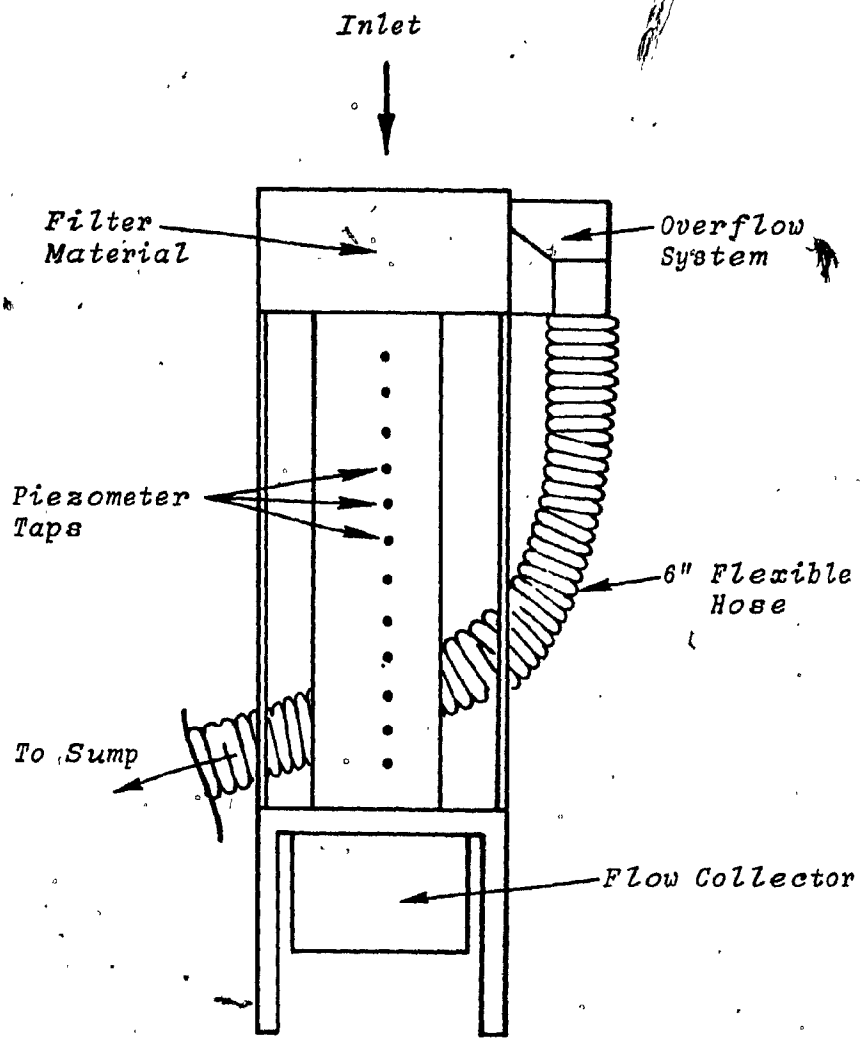

Side View

FIGURE 3.4 (CONTN'D)

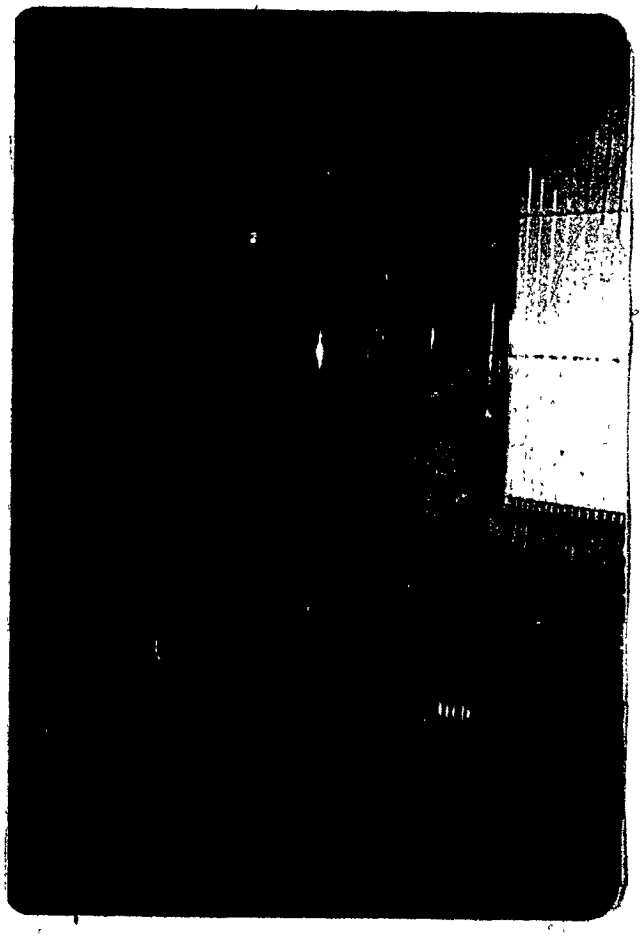

FIGURE 3.5 Parallel Flow Permeameter in Operation

COLOURED PICTURE

FIGURE 3.6 Parallel Flow Permeameter Overflow in Operation

COLOURED PICTURE

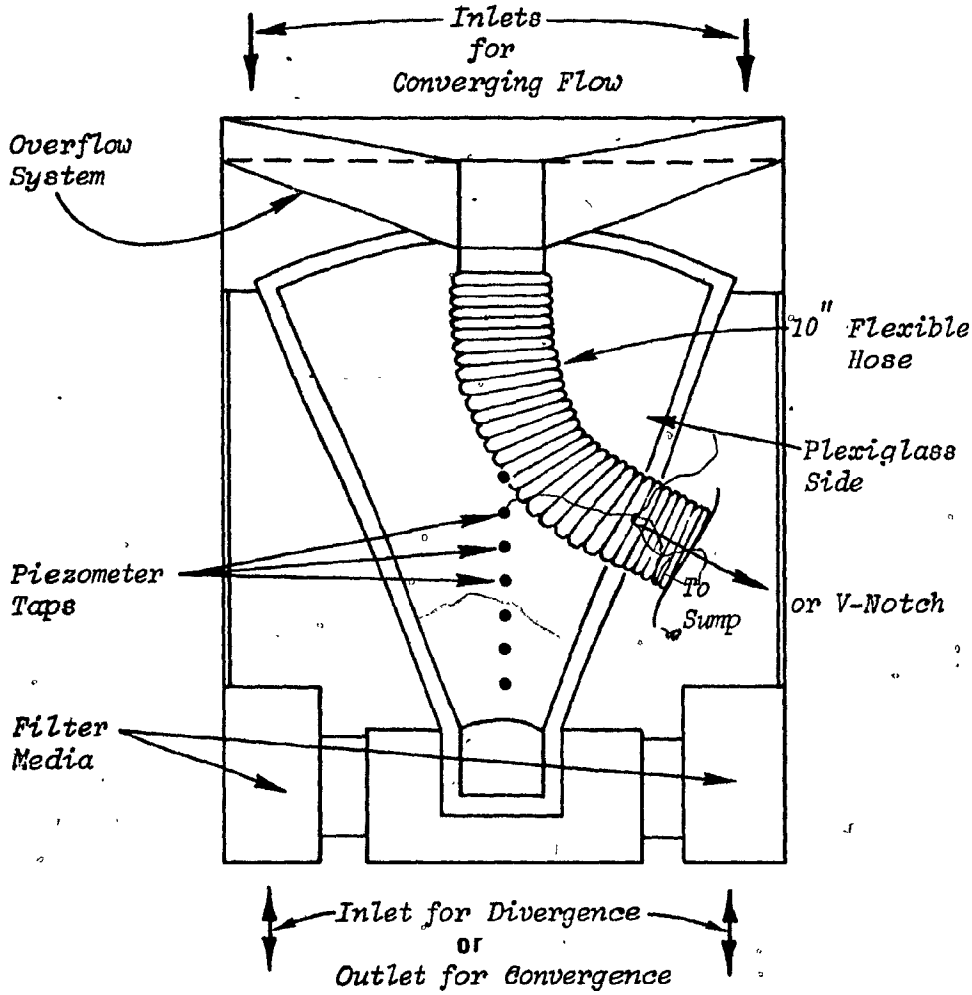

Front View

FIGURE 3.7 Schematic Diagram of the Radial Flow Permeameter

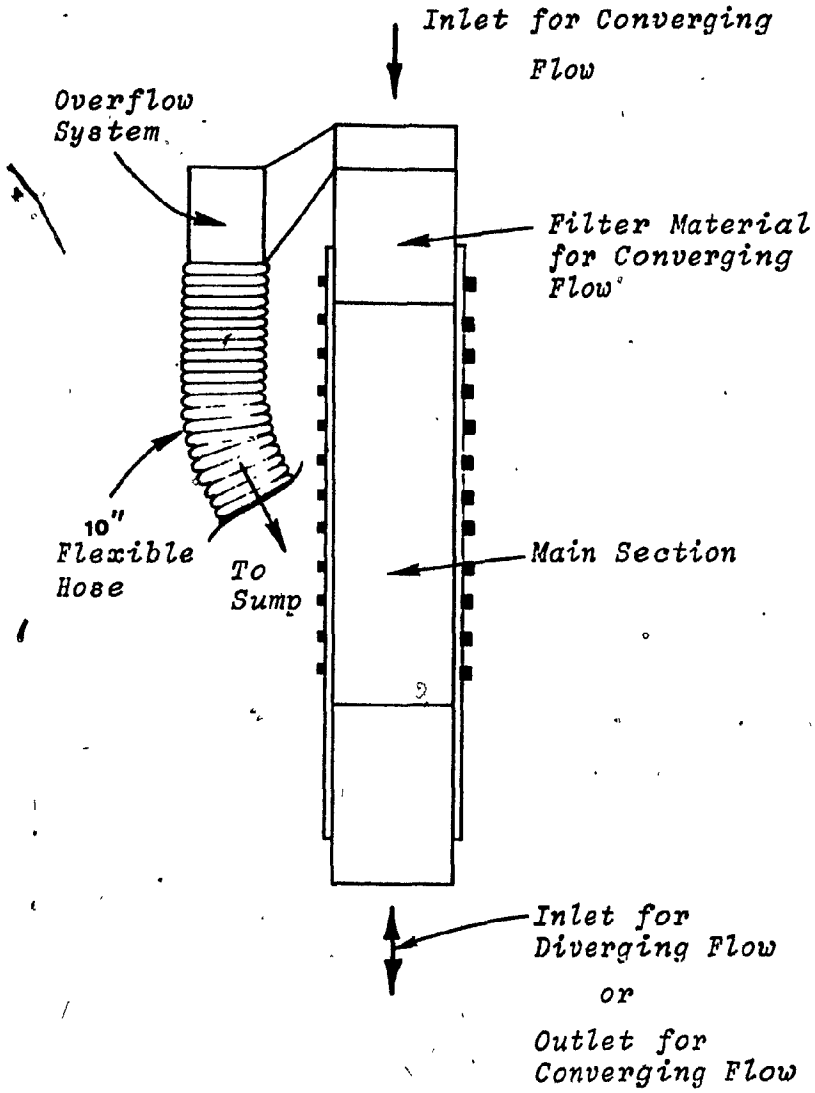

FIGURE 3.7 (CONTN'D)

FIGURE 3.8 Radial Flow Permeameter in Operation

COLOURED PICTURE

FIGURE 3.9 Radial Flow Permeameter Overflow in Operation

COLOURED PICTURE

FIGURE3.10 Laboratory Set-Up

COLOURED PICTURE

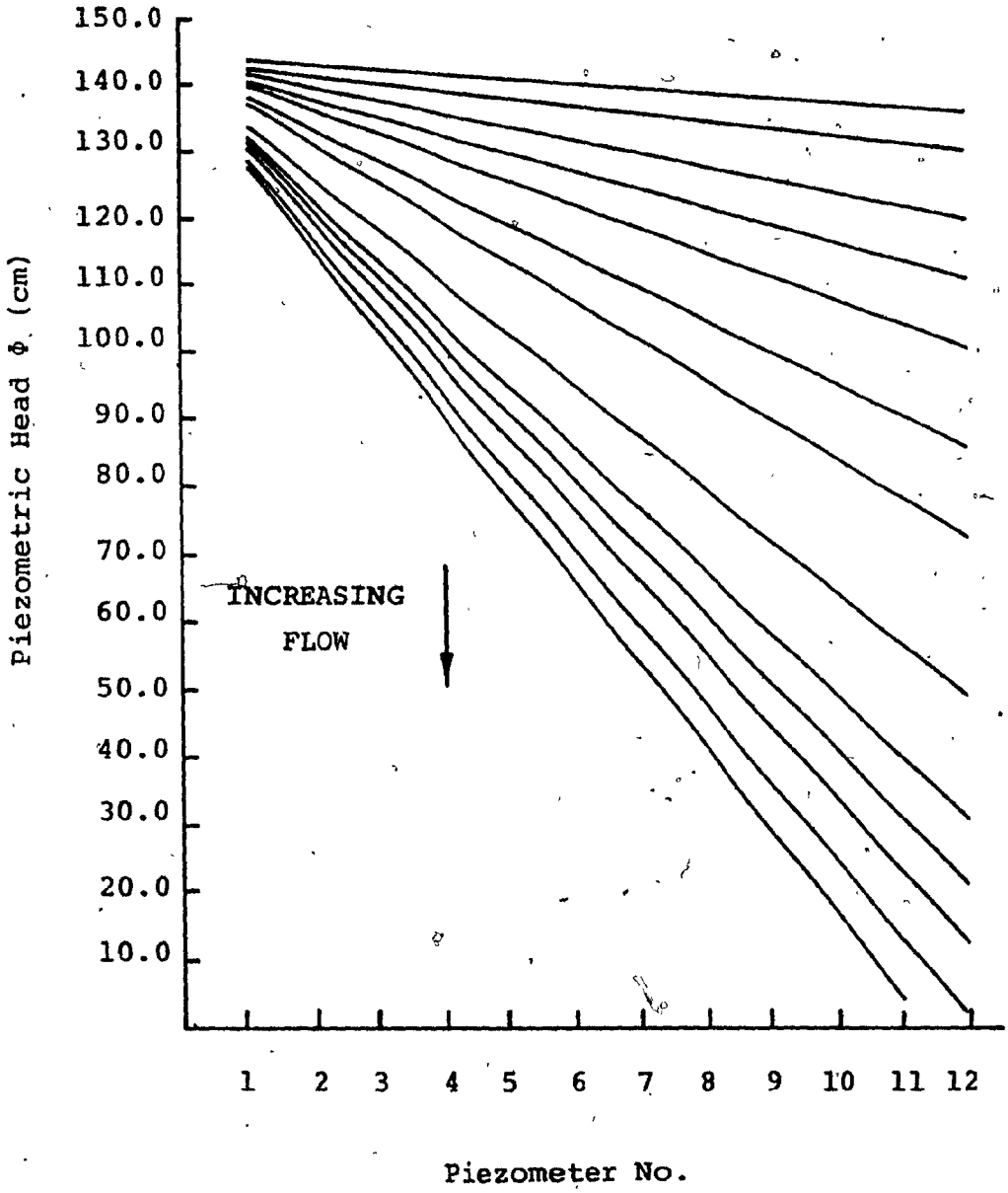

FIGURE 3.11 Piezometric Head vs Location for the 1.51 cm Spheres in the Parallel Flow Permeameter

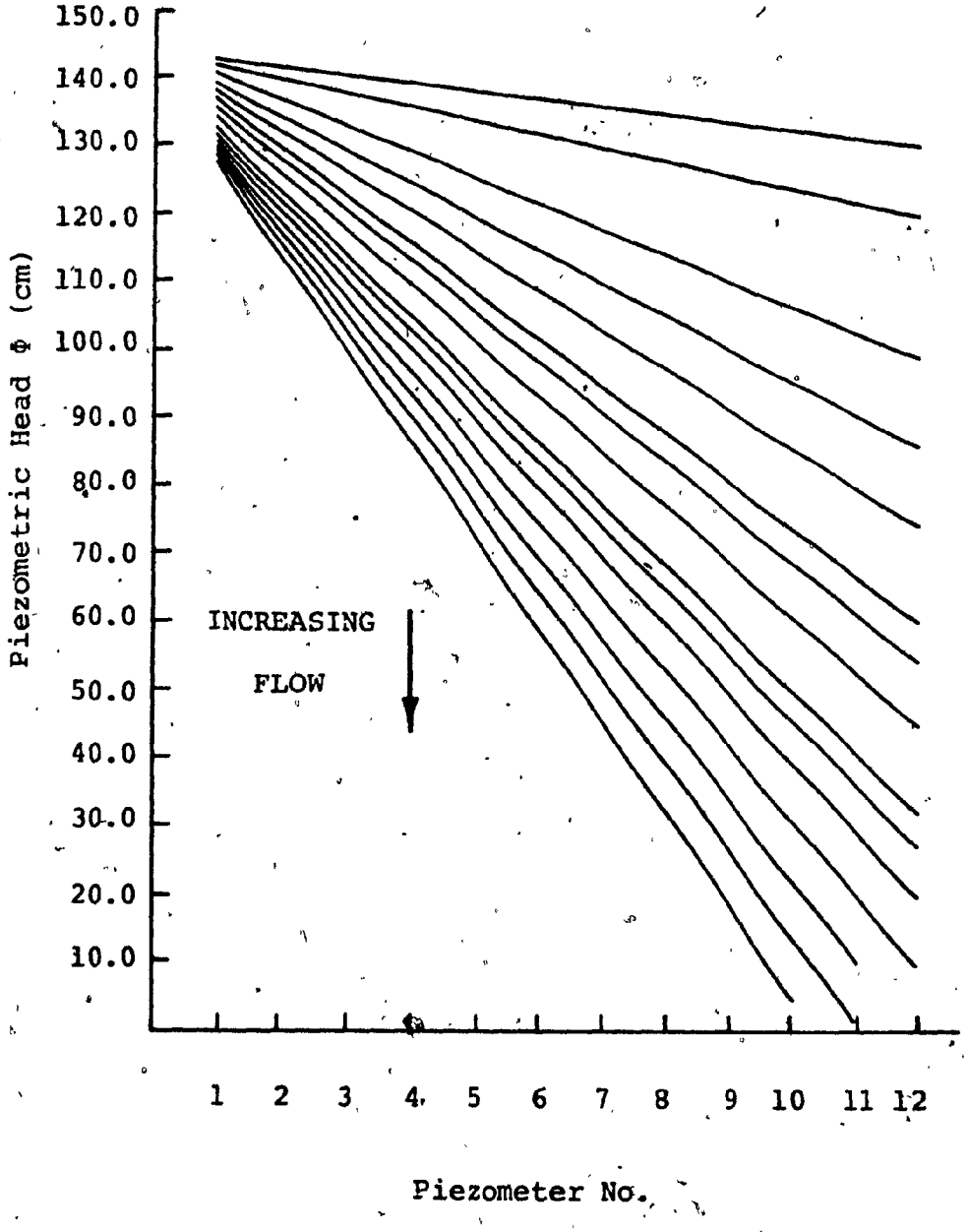

FIGURE 3.12 Piezometric Head vs Location for the 2.06 cm Rocks for the Parallel Flow Permeameter

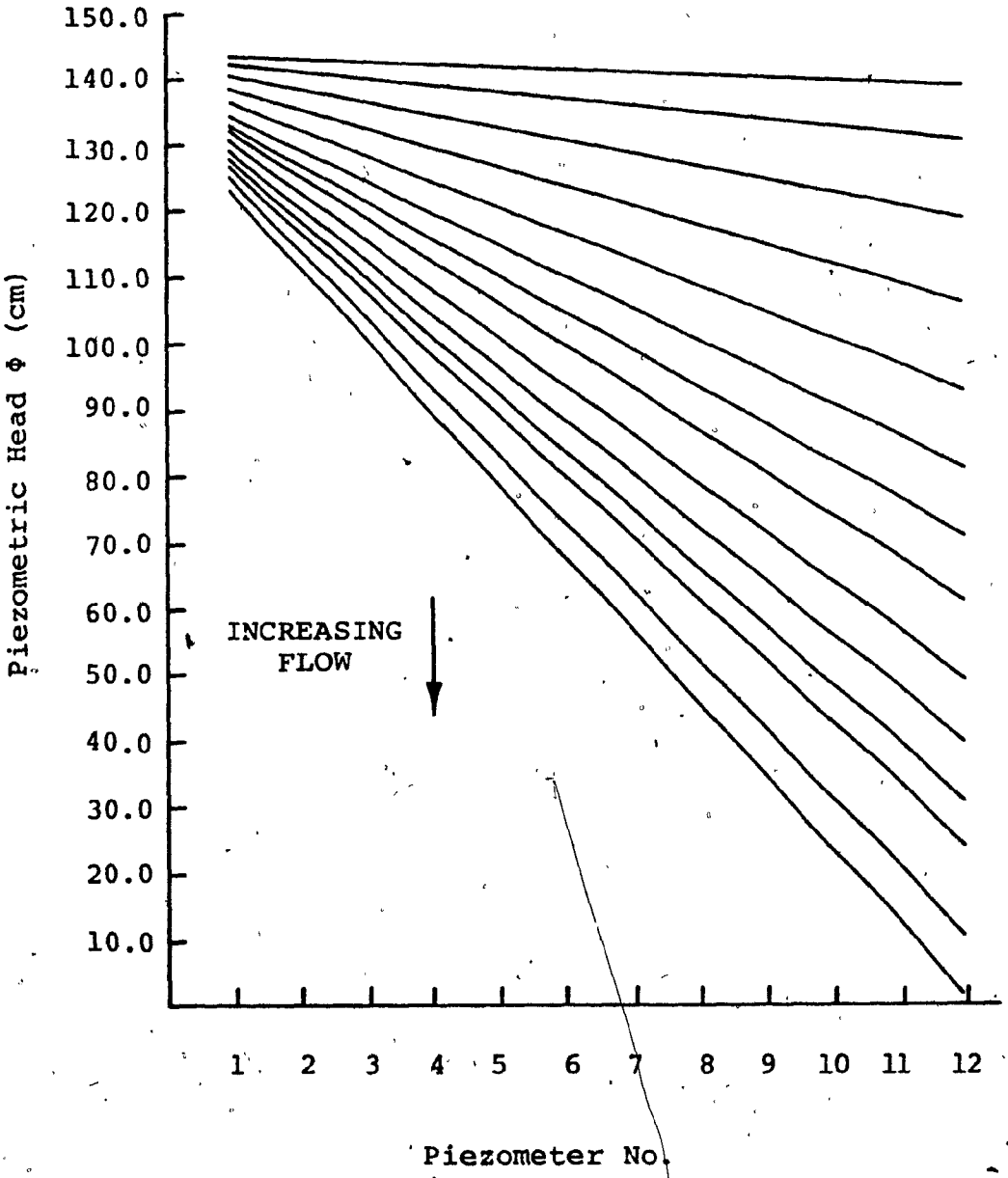

FIGURE 3.13 Piezometric Head vs Location for the 3.16 cm Rocks in the Parallel Flow Permeameter

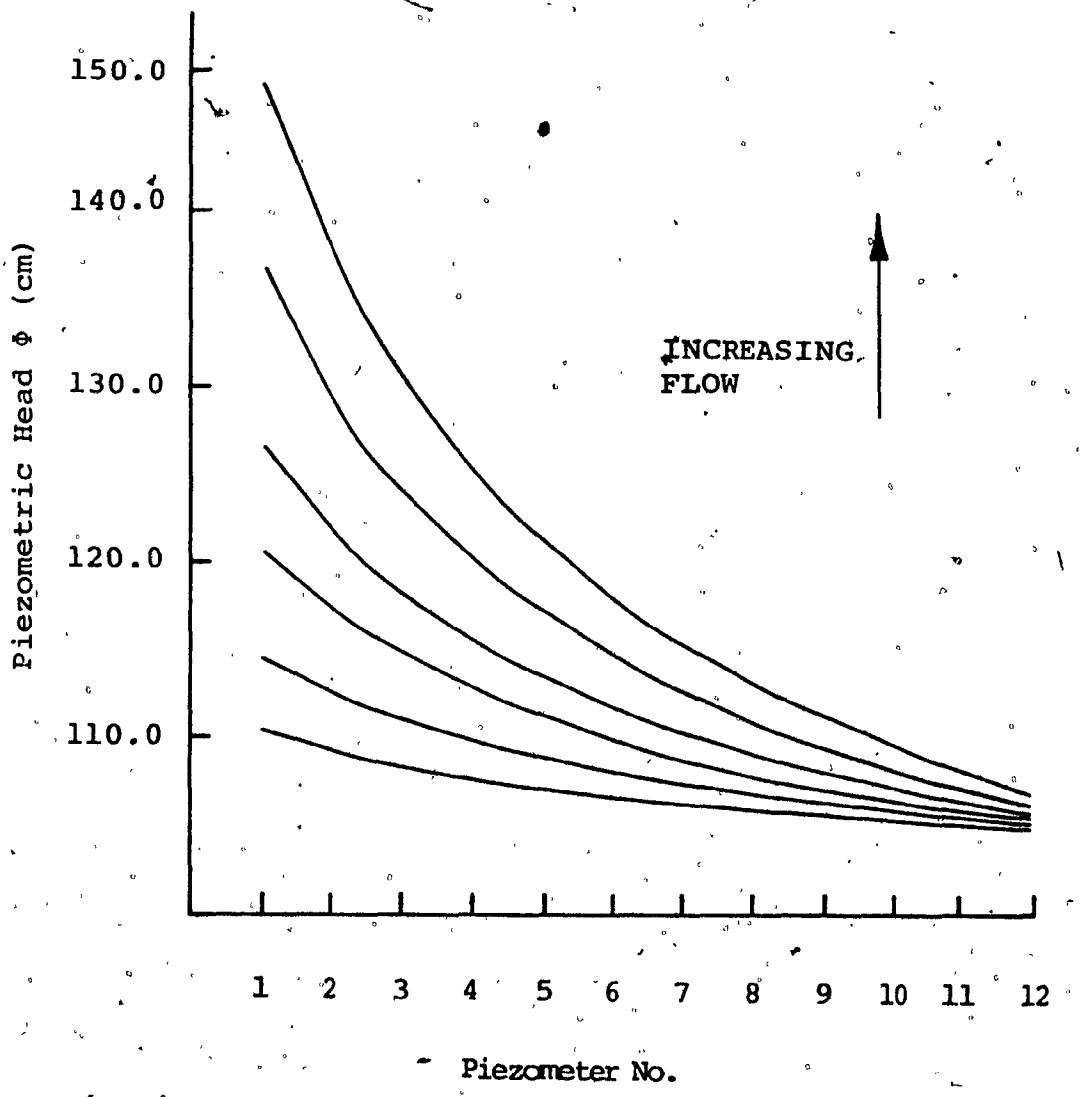

FIGURE 3.14 Piezometric Head vs Radial Distance for the 1.51 cm Spheres in the Diverging Flow Permeameter

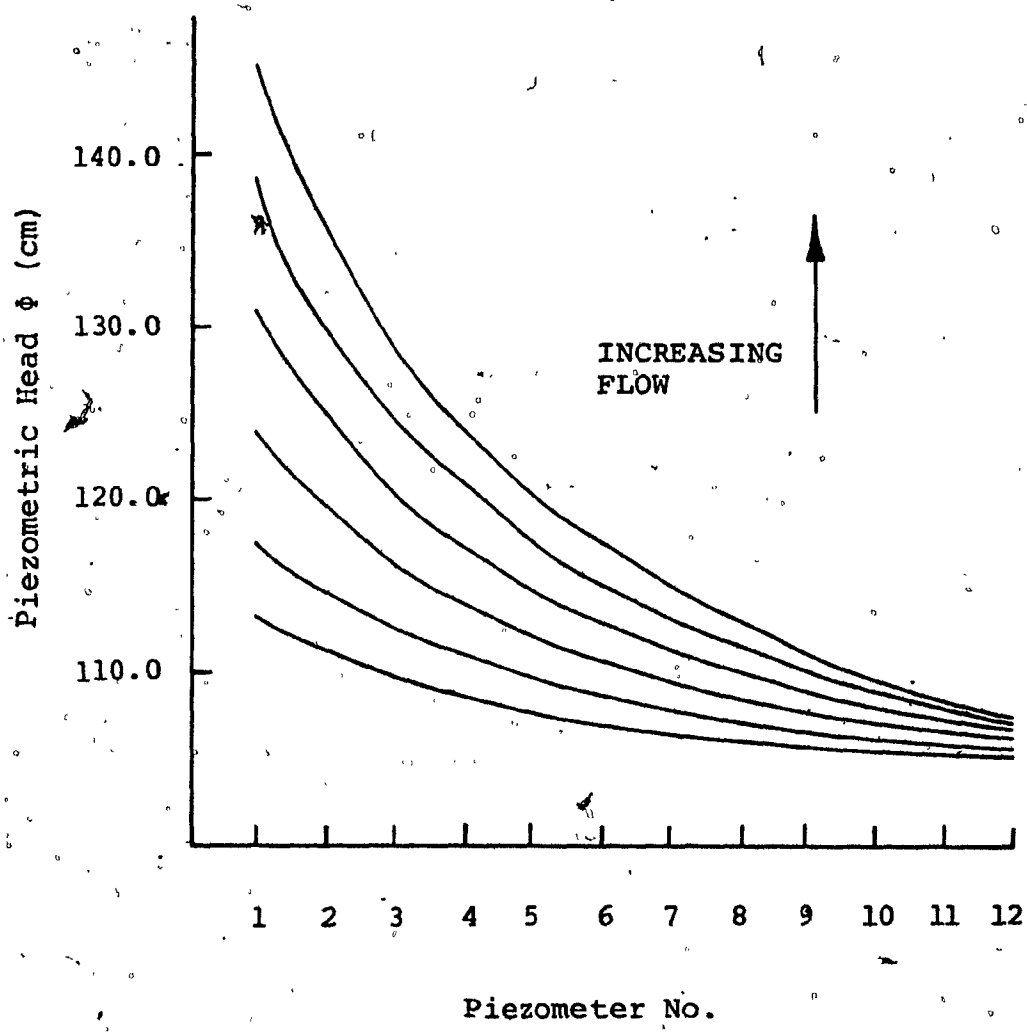

FIGURE 3.15 Piezometric Head vs Radial Distance for the 2.06 cm Rocks in Diverging Flow Permeameter

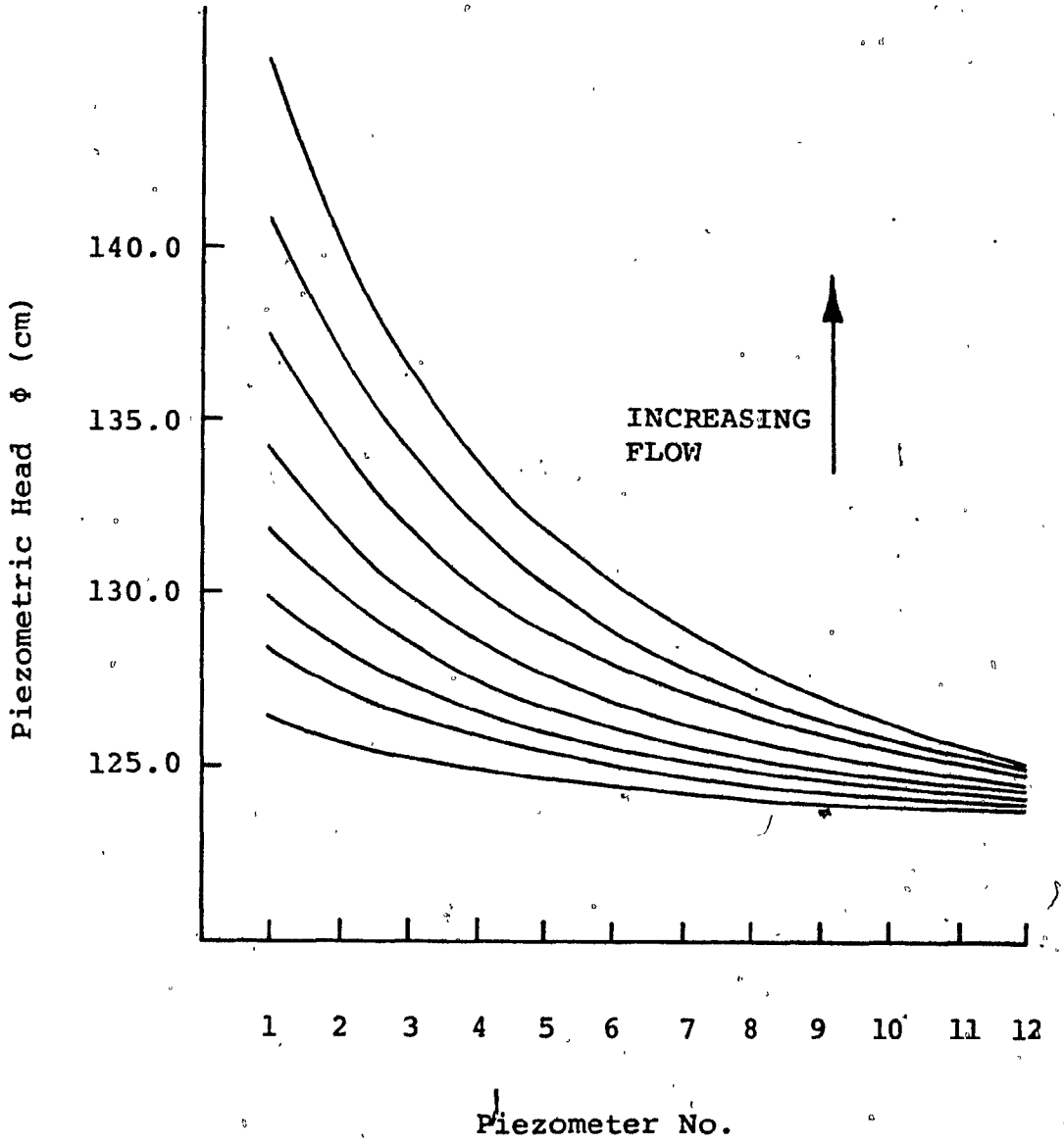

FIGURE 3.16 Piezometric Head vs Radial Distance for the 3.16 cm Rocks in the Diverging Flow Permeameter

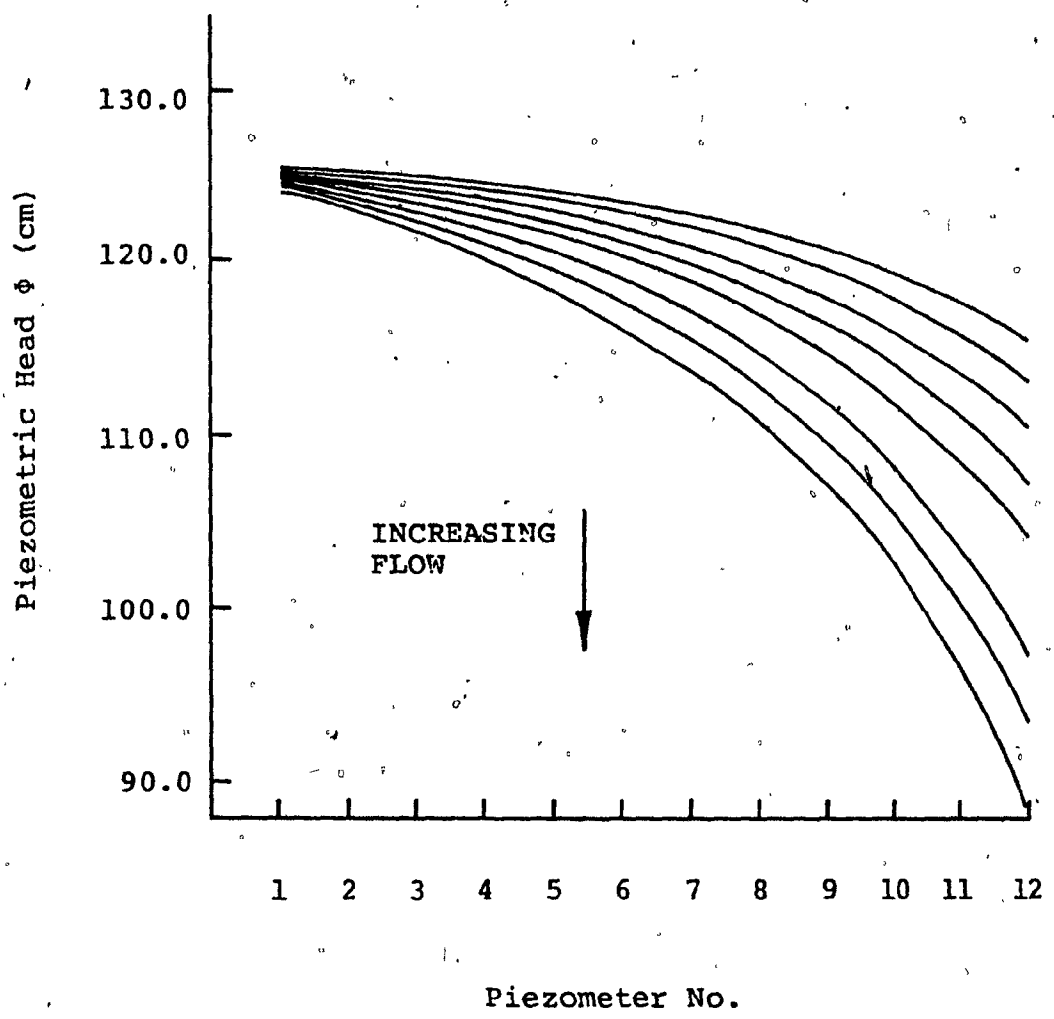

FIGURE 3.17 Piezometric Head vs Radial Distance for the 1.51 cm Spheres in the Converging Flow Permeameter

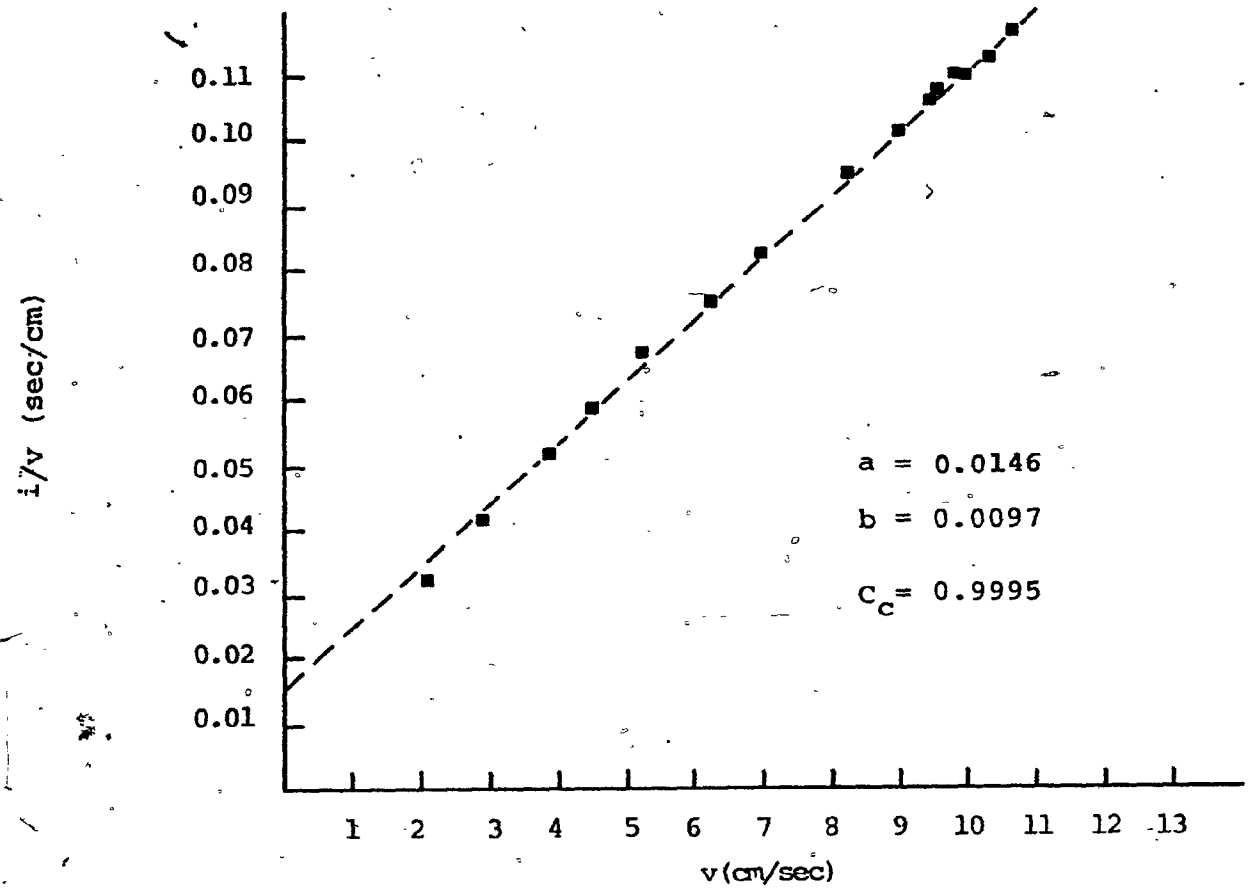

FIGURE 4.3 Parallel Friction Curve for the 1.51 cm Spheres

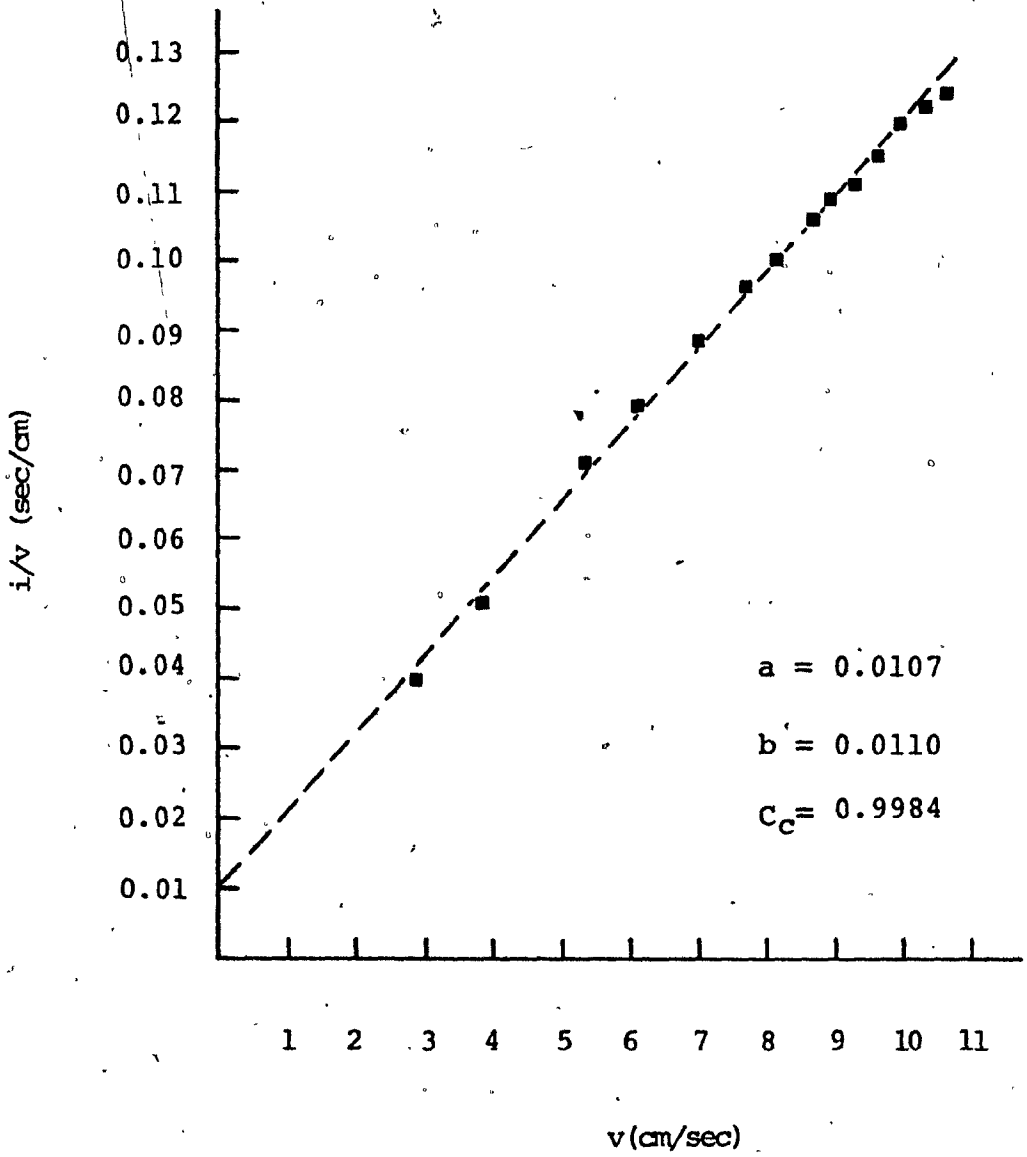

FIGURE 44 Parallel Friction Curve for 2.06 cm Rocks

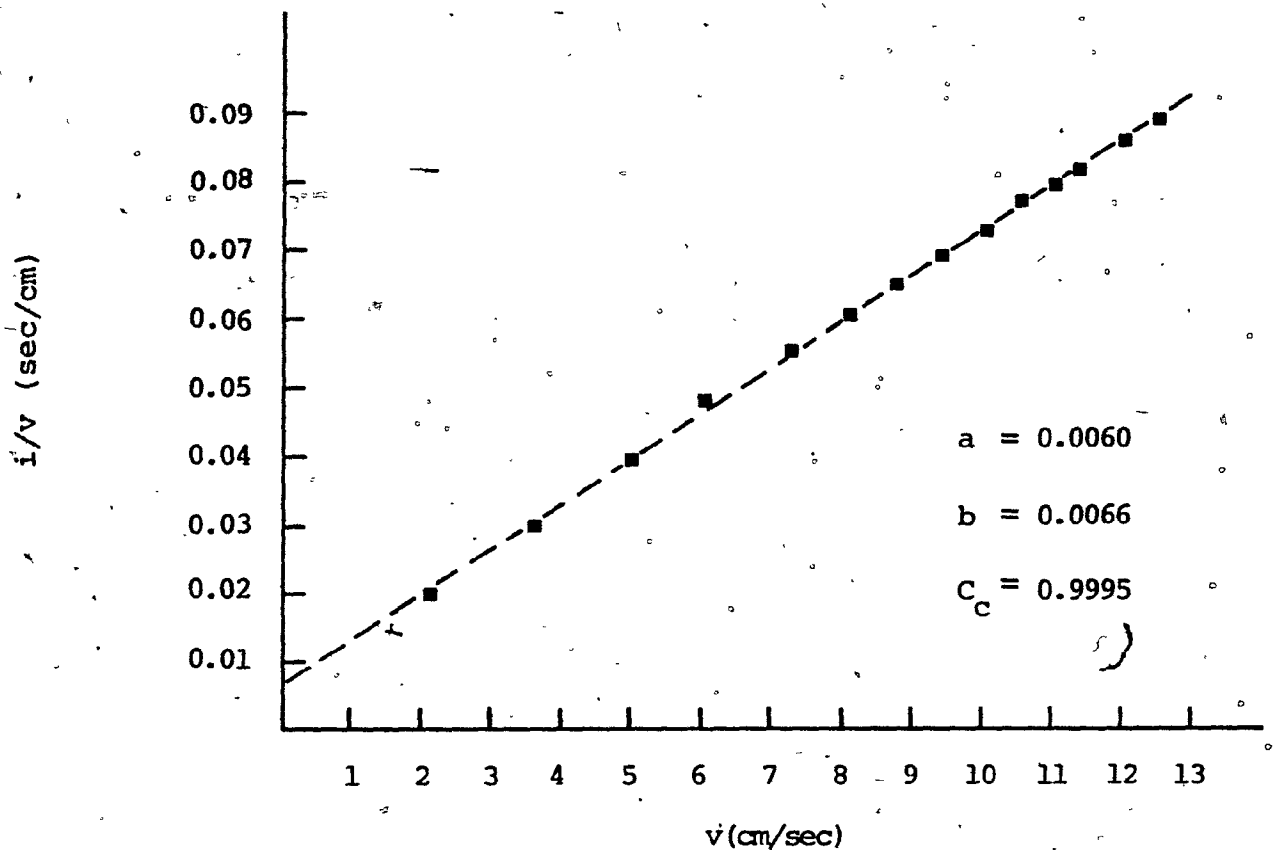

FIGURE 4.5 Parallel Friction Curve for the 3.16 cm Rocks

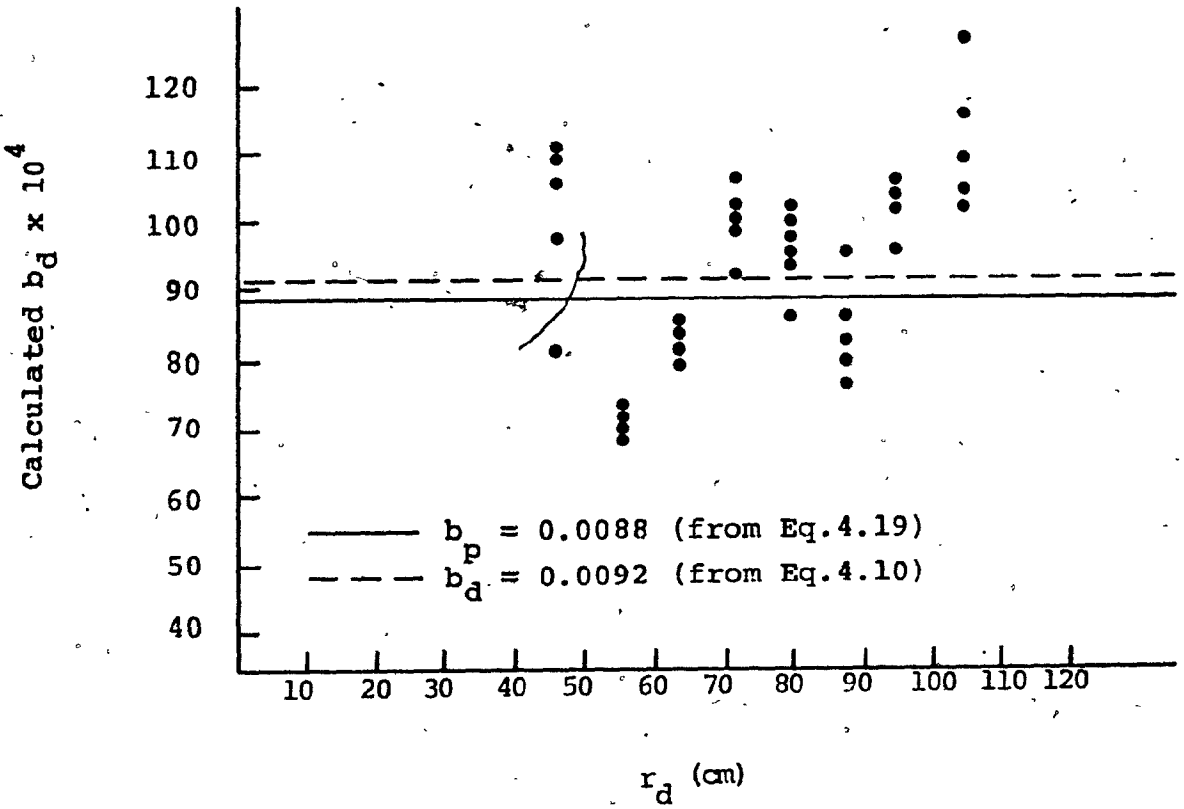

FIGURE 4.6 Scatter Diagram for b_d vs r_d for 1.51 cm Spheres

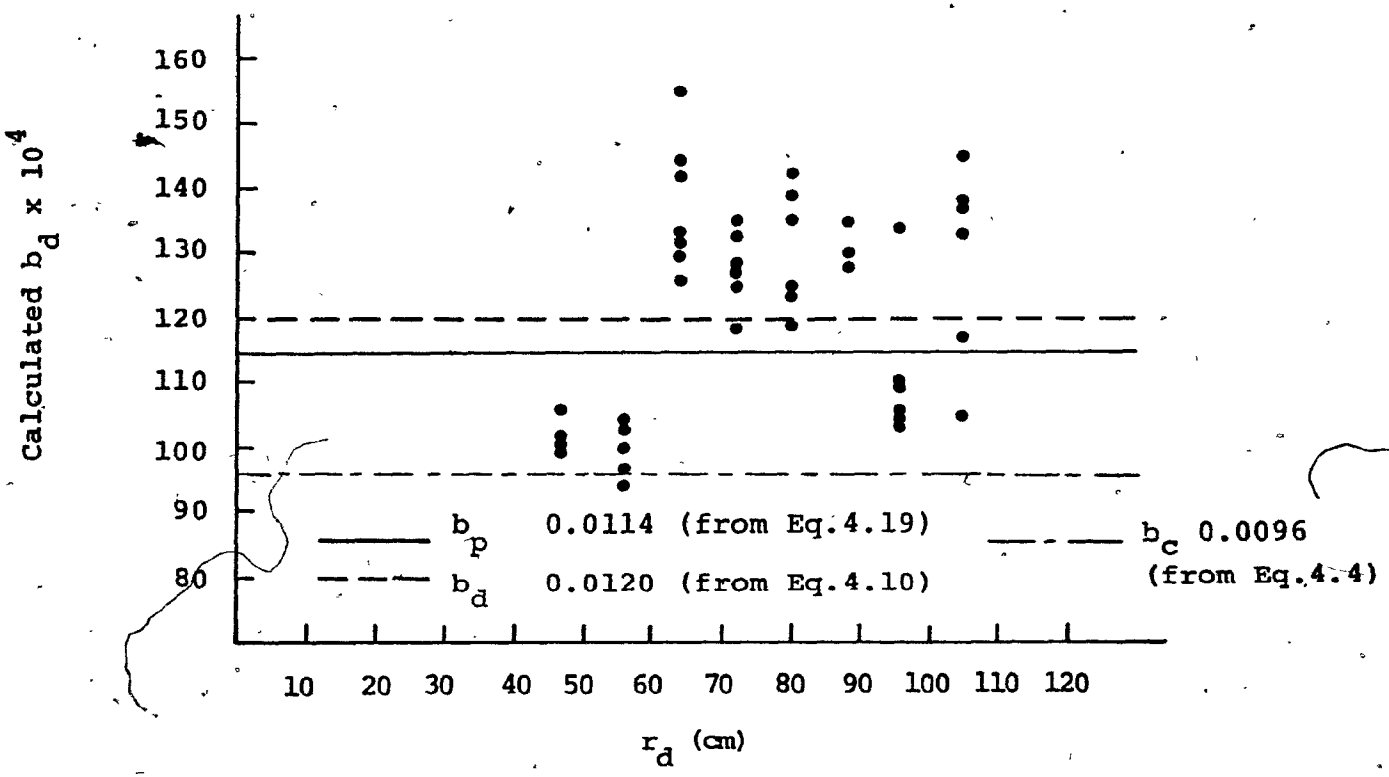

FIGURE 4.7 Scatter Diagram for b_d vs r_d for 2.06 cm Rocks

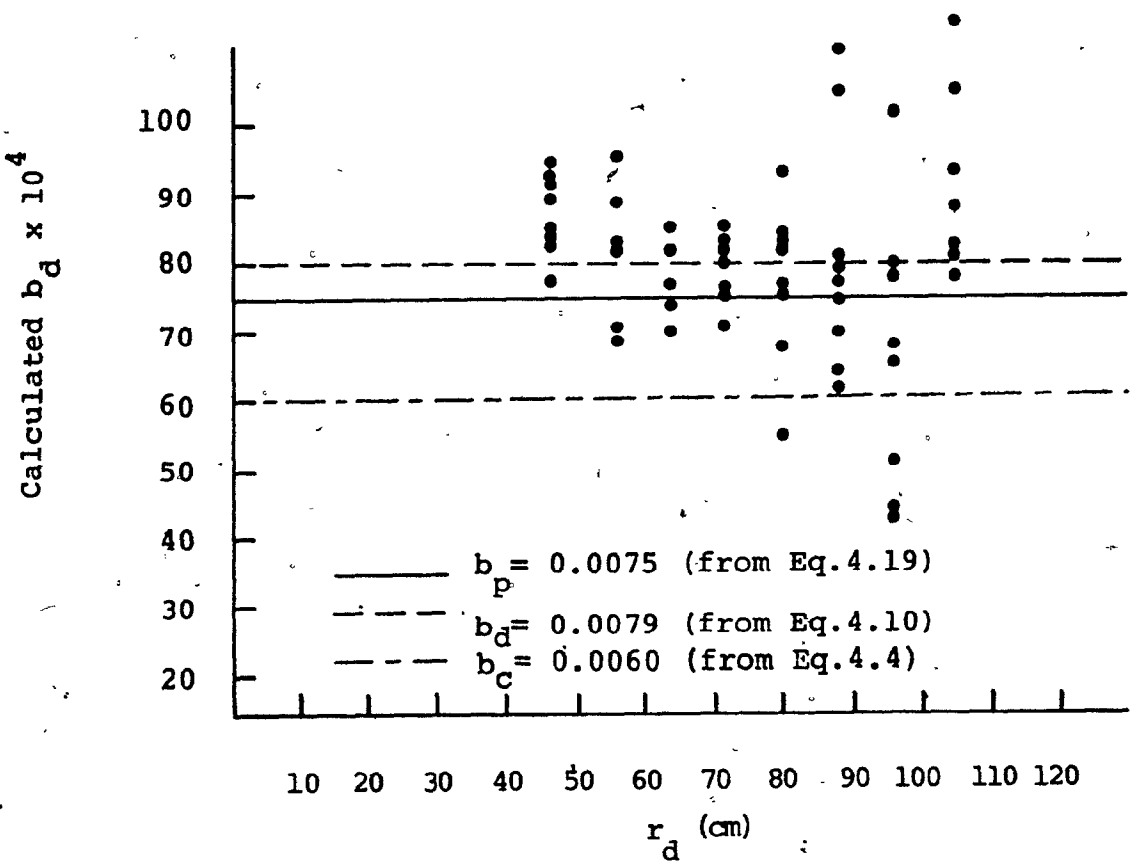

FIGURE 4.8 Scatter Diagram for b_d vs r_d for3.16 cm Rocks

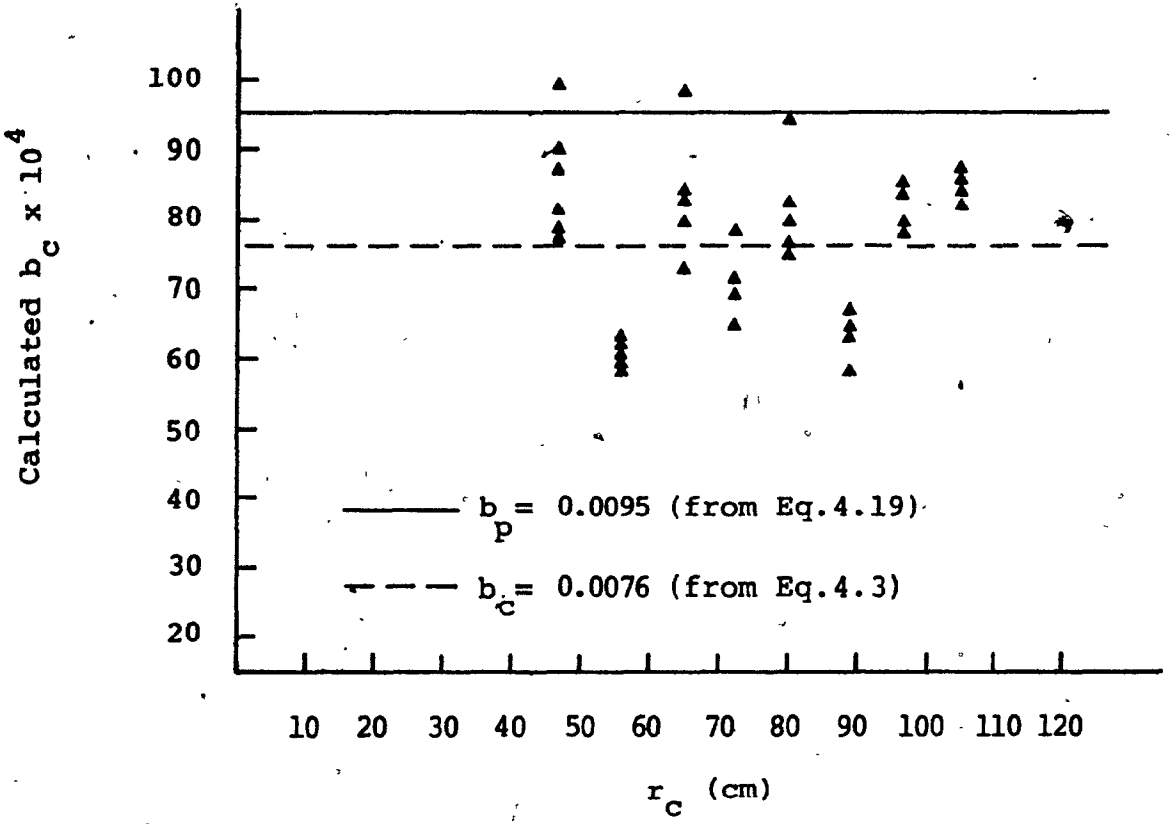

FIGURE 4.9 Scatter Diagram for b_c vs r_c for 1.51 cm Spheres

APPENDIX B

TABLES

TABLE 3.1 Characteristics of the Glass Spheres

Sample No.	Weight (gms) ±0.005	Volume (cm^3) ±0.05	Specific Weight (gm/cm^3)	Nominal Diameter (cm)
1	5.04	2.0	2.52	1.56
2	4.60	1.9	2.42	1.52
3	4.89	2.0	2.45	1.54
4	4.01	1.6	2.51	1.45
5	4.25	1.7	2.50	1.47
6	4.70	1.9	2.47	1.53
7	4.23	1.8	2.35	1.48
8	4.62	1.9	2.43	1.52
9	3.96	1.5	2.64	1.45
10	3.98	1.5	2.65	1.45
11	4.00	1.5	2.67	1.45
12	4.72	1.9	2.48	1.50
13	4.01	1.5	2.67	1.45
14	3.34	1.4	2.39	1.36
15	4.84	1.9	2.55	1.54
16	4.85	1.9	2.55	1.59
17	5.14	2.1	2.45	1.56
18	5.11	2.1	2.43	1.54
19	4.99	2.0	2.50	1.56
20	4.75	1.9	2.54	1.52
	average value ------		2.51 ---	1.51

TABLE 3.2 Characteristics of the Small Rocks

Sample No.	Weight (gms) ±0.005	Volume (cm^3) ±0.05	Specific Weight (gm/cm^3)	Nominal Diameter (cm)
1	12.45	4.6	2.71	2.06
2	39.65	13.5	2.94	2.95
3	13.40	5.2	2.58	2.15
4	10.29	3.9	2.64	1.95
5	11.14	4.2	2.65	2.00
6	9.79	3.6	2.72	1.90
7	7.78	3.1	2.51	1.81
8	5.34	2.1	2.54	1.59
9	11.50	4.7	2.45	2.08
10	9.80	3.4	2.88	1.87
11	7.00	2.9	2.41	1.77
12	7.25	2.8	2.59	1.75
13	8.33	3.7	2.25	1.92
14	18.43	6.7	2.75	2.34
15	11.43	4.5	2.54	2.05
16	21.11	8.5	2.48	2.53
17	31.74	11.0	2.89	2.76
18	6.36	2.4	2.65	1.66
19	9.14	4.1	2.23	1.99
20	11.45	3.3	3.47	1.85

TABLE 3.2 (CONTN'D)

Sample No.	Weight (gms) ±0.005	Volume (cm^3) ±0.05	Specific Weight (gm/cm^3)	Nominal Diameter (cm)
21	19.85	7.6	2.61	2.44
22	14.75	5.7	2.59	2.22
23	27.00	11.5	2.35	2.80
24	8.70	3.1	2.81	1.59
25	14.70	6.7	2.19	2.34
26	11.77	4.4	2.68	2.03
27	15.25	4.8	3.18	2.09
28	12.80	4.3	2.98	2.02
29	9.91	3.5	2.83	1.79
30	8.55	3.2	2.67	2.19
	average value ------		2.66 ---	2.06

TABLE 3.3 Characteristics of the Large Rocks

Sample No.	Weight (gms) ±0.005	Volume (cm^3) ±0.5	Specific Weight (gm/cm^3)	Nominal Diameter (cm)
1	59.95	21.5	2.79	3.92
2	32.87	13.5	2.43	2.95
3	51.31	18.5	2.77	3.28
4	56.72	20.5	2.77	3.40
5	63.69	24.5	3.60	2.60
6	62.31	21.0	2.97	3.42
7	88.48	32.5	2.72	3.96
8	66.95	23.5	2.85	3.55
9	37.13	15.5	2.40	3.09
10	40.38	15.5	2.61	3.09
11	49.78	18.0	2.77	3.25
12	86.77	30.0	2.89	3.86
13	64.79	26.5	2.44	3.70
14	23.60	9.0	2.62	2.58
15	70.00	24.5	2.86	3.60
16	34.90	12.5	2.88	2.79
17	42.10	15.5	2.72	3.09
18	46.76	19.5	2.40	3.34
19	36.11	14.0	2.58	2.99
20	33.98	12.0	2.83	2.84

TABLE 3.3 (CONTN'D)

Sample No.	Weight (gms) ±0.005	Volume (cm^3) ±0.5	Specific Weight (gm/cm^3)	Nominal Diameter (cm)
21	30.28	12.0	2.52	2.84
22	23.81	9.5	2.51	2.63
23	25.75	9.5	2.71	2.63
24	59.59	21.0	2.84	3.42
25	57.54	21.0	2.74	3.42
26	27.52	10.5	2.62	2.53
27	32.05	11.0	2.91	2.76
28	58.31	23.0	2.54	3.53
29	26.80	9.5	2.82	2.53
30	39.75	14.5	2.74	3.03
	average value ----		2.69 ---	3.16

TABLE 3.4 Characteristics of the Three Porous Media

	Spheres	Small Rocks	Large Rocks
Specific Weight (gm/cm^3) γ_m	2.51	2.66	2.69
Nominal Diameter D_m	1.51	2.06	3.16
Shape Factor λ_s	6.0	10.2 (estimated)	9.5 (estimated)

TABLE 3.5 In-Situ Porosity Values for the Three porous Media

	Spheres	Small Rocks	Large Rocks
Porosity in Parallel Permeameter	0.37	0.41	0.40
Porosity in Converging Permeameter	0.385	-	-
Porosity in Diverging Permeameter	0.40	0.42	0.40

TABLE 3.6 Parallel Flow Data for 1.51 cm Glass Spheres

Temperature 22.2 °C

Flow(lps)			6.00	6.48	6.31	5.80	5.52	5.04	4.28	3.82
Piez. No.	L (cm)	Test #	1	2	3	4	5	6	7	8
1	12.0		130.4	128.0	129.1	131.3	132.5	134.3	137.1	138.4
2	22.0		120.1	116.3	117.9	121.7	123.6	127.0	131.4	134.0
3	32.0		109.9	104.9	107.1	112.3	115.0	119.8	126.1	129.4
4	42.0		100.3	94.2	96.6	103.5	106.9	112.9	121.0	125.3
5	52.0		89.9	81.8	85.3	93.5	97.9	105.1	115.2	120.6
6	62.0		77.3	67.1	71.5	81.6	87.2	96.8	108.3	115.0
7	72.0		66.4	54.9	60.0	71.6	78.0	88.0	102.4	110.2
8	82.0		56.3	43.2	49.0	62.0	69.2	81.0	97.1	105.9
9	92.0		45.6	31.5	37.9	52.6	60.3	73.4	91.6	101.2
10	102.0		31.9	15.5	22.7	39.5	48.4	63.4	84.2	95.0
11	112.0		22.4	4.3	12.0	30.4	40.0	56.4	78.9	90.6
12	122.0		11.9	-	0.5	20.6	31.2	48.6	73.3	86.1

TABLE 3.6 (CONTN'D)

Flow(lps)			3.23	2.78	2.35	1.76	1.27
Piez. No.	L (cm)	Test #	9	10	11	12	13
1	12.0		140.0	141.1	142.1	143.3	144.0
2	22.0		136.7	138.7	140.4	142.2	143.5
3	32.0		133.4	136.2	138.5	140.9	142.7
4	42.0		130.2	133.4	136.6	139.8	142.0
5	52.0		126.9	131.1	134.7	138.8	141.5
6	62.0		122.8	127.8	132.3	137.5	140.6
7	72.0		119.4	125.2	130.2	136.2	140.0
8	82.0		115.9	123.0	128.4	135.1	139.3
9	92.0		112.4	120.0	126.4	133.8	138.7
10	102.0		107.8	116.6	123.8	132.2	137.8
11	112.0		104.5	114.0	121.9	131.1	137.2
12	122.0		101.2	111.6	120.0	130.0	136.5

TABLE 3.7 Parallel Flow Data for 2.06 cm Rocks
Temperature 23.3 °C

Flow(lps)			1.75	2.39	3.25	3.77	4.18	4.31	4.78	5.03
Piez No.	L (cm)	Test #	1	2	3	4	5	6	7	8
1	12.0		142.6	141.1	140.6	139.4	138.0	137.5	135.8	134.8
2	22.0		141.5	139.2	137.0	134.1	131.7	130.9	127.8	125.9
3	32.0		140.4	137.6	133.5	130.0	126.8	125.7	121.4	118.7
4	42.0		139.1	135.0	129.0	124.3	120.0	118.4	112.6	109.2
5	52.0		137.8	132.4	124.4	118.3	112.8	110.8	103.4	98.8
6	62.0		136.8	130.9	121.3	114.2	108.0	105.7	97.4	92.2
7	72.0		135.2	128.2	116.1	107.5	100.0	97.2	87.1	80.8
8	82.0		133.8	125.7	111.6	101.6	93.0	89.7	78.2	71.2
9	92.0		132.8	124.1	108.8	98.3	88.6	85.0	72.6	65.2
10	102.0		131.8	122.5	105.8	94.3	83.8	80.2	66.8	58.7
11	112.0		131.0	120.7	102.8	90.4	79.2	75.2	60.6	52.3
12	122.0		130.0	119.0	98.7	86.0	74.2	69.8	54.0	44.6

TABLE 3.7 (CONTN'D)

Flow(lps)			5.36	5.48	5.71	5.94	6.14	6.39	6.52
Piez No.	L (cm)	Test #	9	10	11	12	13	14	15
1	12.0		133.4	132.8	132.0	130.8	129.8	128.8	128.0
2	22.0		123.6	122.6	121.0	119.0	117.2	115.5	114.2
3	32.0		115.7	114.4	112.3	109.4	107.0	104.5	102.7
4	42.0		105.0	103.3	100.4	96.4	93.2	89.7	87.2
5	52.0		93.5	91.2	87.3	82.3	78.2	73.3	70.2
6	62.0		86.0	83.5	79.1	73.4	68.6	63.4	59.8
7	72.0		73.2	70.1	65.0	58.2	52.0	45.9	41.3
8	82.0		62.0	59.0	53.0	45.4	37.8	30.6	25.6
9	92.0		55.5	51.8	45.1	36.8	29.0	21.5	15.9
10	102.0		48.1	44.0	36.4	26.2	19.5	10.9	5.0
11	112.0		40.3	36.5	28.6	18.5	10.0	1.0	-
12	122.0		32.0	27.4	19.2	8.5	-	-	-

TABLE 3.8 Parallel Flow Data for 3.16 cm Rocks
Temperature 23.3 °C

Flow(lps)			1.28	2.25	3.11	3.77	4.47	5.00	5.40	5.82
Piez. No.	L (cm)	Test #	1	2	3	4	5	6	7	8
1	12.0		143.3	142.2	140.4	138.7	136.5	134.8	133.2	132.3
2	22.0		143.0	141.2	138.6	135.9	132.6	130.0	127.6	125.9
3	32.0		142.5	140.2	136.9	133.2	129.2	125.6	122.6	120.2
4	42.0		142.2	139.2	135.0	130.6	125.6	121.2	117.4	114.2
5	52.0		141.6	138.1	132.6	127.3	121.0	115.5	110.8	106.4
6	62.0		141.1	136.7	130.2	124.0	116.4	110.0	104.0	99.2
7	72.0		140.6	135.6	128.1	120.7	111.6	104.4	97.8	91.7
8	82.0		140.2	134.2	125.8	117.5	107.5	99.1	91.7	84.8
9	92.0		139.8	133.0	123.7	114.4	103.4	94.0	85.6	78.0
10	102.0		139.6	132.2	122.3	112.4	100.4	90.2	81.4	73.1
11	112.0		139.3	131.1	120.3	109.3	96.2	85.2	75.2	66.3
12	122.0		138.9	130.1	118.6	106.7	92.7	80.8	70.2	60.6

TABLE 3.8 (CONTN'D)

Flow(lps)			6.23	6.56	6.86	7.03	7.48	7.71
Piez. No.	L (cm)	Test #	9	10	11	12	13	14
1	12.0		130.6	129.0	128.0	127.0	125.0	123.6
2	22.0		123.2	121.0	119.0	117.4	114.6	112.6
3	32.0		116.9	114.0	111.4	109.5	105.8	103.1
4	42.0		109.8	106.6	103.2	101.0	96.3	93.0
5	52.0		101.4	96.6	93.0	90.0	84.0	79.8
6	62.0		92.8	87.1	82.8	79.0	72.0	66.9
7	72.0		84.4	77.8	73.0	68.6	60.4	54.3
8	82.0		76.4	69.0	63.8	58.7	49.4	42.9
9	92.0		68.7	60.4	54.5	49.0	38.6	31.0
10	102.0		63.2	55.2	48.3	41.0	30.8	22.7
11	112.0		55.2	46.3	38.5	32.0	19.8	11.0
12	122.0		49.0	39.2	30.9	24.0	10.6	1.4

TABLE 3.9 Diverging Flow Data for 1.51 cm Spheres
Temperature 24.4 °C

Flow (lps)		3.35			4.54			5.98			6.097		
Piez. No.	Test #	1			2			3			4		
	r_d (cm)	A	B	ave.	A	B	ave.	A	B	ave.	A	B	ave.
1	35.00	110.4	110.4	110.4	114.5	114.3	114.4	120.5	120.2	120.35	126.6	127.2	126.9
2	43.25	109.1	109.4	109.25	112.2	112.6	112.4	116.8	117.5	117.15	121.4	121.1	121.25
3	51.50	108.1	108.1	108.1	110.6	110.6	110.6	114.2	114.2	114.2	117.8	118.1	117.95
4	59.75	107.6	107.6	107.6	109.6	109.6	109.6	112.6	112.7	112.65	115.7	115.8	115.75
5	68.00	107.2	107.0	107.1	108.8	108.7	108.75	111.4	111.1	111.25	114.0	113.5	113.75
6	76.25	106.6	106.7	106.65	108.0	108.0	108.0	109.8	110.0	109.9	111.9	112.0	111.95
7	84.50	106.3	106.2	106.25	107.4	107.4	107.4	108.8	108.9	108.85	110.6	110.4	110.5
8	92.75	106.0	106.0	106.0	106.8	106.9	106.85	108.0	108.2	108.1	109.3	109.5	109.4
9	101.0	105.6	105.7	105.65	106.3	106.4	106.35	107.3	107.4	107.35	108.2	108.4	108.3
10	109.25	105.3	105.4	105.35	105.8	105.9	105.85	106.6	106.6	106.6	107.3	107.3	107.3
11	117.50	105.1	105.2	105.15	105.5	105.6	105.55	106.0	106.2	106.1	106.5	106.8	106.65
12	124.75	105.0	105.1	105.05	105.2	105.2	105.2	105.5	105.5	105.5	105.8	105.8	105.8

TABLE 3.9 (CONTN'D)

Flow(lps)		8.86			10.35		
Piez. No.	Test #	5			6		
	r d(cm)	A	B	ave.	A	B	ave.
1	35.00	136.2	137.6	136.9	146.3	148.0	147.15
2	43.25	128.5	129.2	128.85	137.7	137.0	137.35
3	51.50	123.1	123.5	123.3	129.1	129.7	129.40
4	59.75	120.2	120.3	120.25	125.1	125.2	125.15
5	68.00	117.8	117.1	117.45	121.9	121.0	121.45
6	76.25	114.7	115.0	114.85	117.9	118.1	117.95
7	84.50	112.8	112.6	112.7	115.3	115.2	115.25
8	92.75	111.1	111.3	111.2	113.0	113.3	113.15
9	101.0	109.5	109.7	109.6	111.0	111.2	111.1
10	109.25	108.3	108.2	108.25	109.3	109.3	109.3
11	117.50	107.1	107.4	107.25	107.7	108.1	107.9
12	124.75	106.1	106.1	106.1	106.5	106.4	106.45

TABLE 3.10 Diverging Flow Data for 2.06 cm Rocks
Temperature 23.6 °C

Flow(lps)		5.71			5.91			6.20			6.53		
Piez.	Test #	1			2			3			4		
No.	r_d(cm)	A	B	ave	A	B	ave	A	B	ave	A	B	ave
1	35.00	146.0	145.2	145.5	138.6	138.4	138.5	131.2	130.8	131.0	124.0	123.7	123.85
2	43.25	133.8	134.9	134.35	129.0	129.6	129.3	123.6	124.1	123.85	118.5	118.9	118.7
3	51.50	129.1	128.2	128165	125.1	124.2	124.65	120.5	120.0	120.25	116.3	116.0	116.15
4	59.75	124.4	123.6	124.5	122.0	120.6	121.3	118.4	117.1	117.75	114.7	113.8	114.25
5	68.00	121.0	120.5	120.75	118.3	117.8	118.05	115.4	114.9	115.15	112.4	112.1	112.25
6	76.25	117.3	117.6	117.45	115.2	115.4	115.3	113.1	113.2	113.15	110.8	110.8	110.8
7	84.50	114.8	115.0	114.9	113.1	113.3	113.2	111.3	111.4	111.35	109.5	109.6	109.55
8	92.75	112.6	112.8	112.7	111.3	111.5	111.4	109.9	110.0	109.95	108.5	108.5	108.5
9	101.00	111.3	111.0	111.15	110.2	109.9	110.05	109.0	108.8	108.9	107.9	107.6	107.75
10	109.25	109.5	109.4	109.45	108.7	108.6	108.65	107.9	107.8	107.85	107.1	107.0	107.05
11	117.50	108.4	108.3	108.35	107.8	107.7	107.75	107.2	107.2	107.2	106.6	106.5	106.55
12	125.75	107.4	107.3	107.35	107.0	107.0	107.0	106.6	106.6	106.6	106.2	106.1	106.15

TABLE 3.10 (CONTN'D)

Flow(lps)		6.92			7.28		
Piez. No.	Test #	5			6		
	r_d (cm)	A	B	ave	A	B	ave
1	35.00	117.7	117.3	117.5	113.3	113.0	113.15
2	43.25	115.9	114.1	114.0	110.7	110.8	110.75
3	51.50	112.4	112.2	112.3	109.7	109.5	109.6
4	59.75	111.3	110.7	111.0	109.0	108.5	108.75
5	68.00	109.8	109.6	109.7	108.0	107.8	107.9
6	76.25	108.8	108.7	108.75	107.3	107.2	107.25
7	84.50	107.9	107.9	107.9	106.7	106.8	106.75
8	92.75	107.2	107.2	107.2	106.2	106.2	106.2
9	101.00	106.8	106.6	106.7	105.9	105.7	105.8
10	109.25	106.2	106.1	106.15	105.6	105.4	105.5
11	117.50	105.9	105.7	105.8	105.4	105.2	105.3
12	125.75	105.6	105.6	105.6	105.2	105.1	105.15

TABLE 3.11 Diverging Flow Data for 3.16 cm Rocks
Temperature 22.7 °C

Flow(lps)		7.92			6.87			6.06			5.25		
Piez. No.	Test #	1			2			3			4		
	r_d(cm)	A	B	ave	A	B	ave	A	B	ave	A	B	ave
1	35.00	145.6	145.5	145.55	141.1	140.9	141.0	137.6	137.6	137.6	134.3	134.2	134.25
2	43.25	140.6	140.3	140.45	137.0	136.6	136.8	134.5	134.0	134.25	131.8	131.6	131.7
3	51.50	136.8	136.6	136.7	134.1	133.8	133.95	132.0	131.6	131.8	130.1	129.6	129.05
4	59.75	133.4	134.2	133.8	131.6	131.9	131.75	130.0	130.3	130.15	128.5	128.7	128.65
5	68.00	132.0	131.8	131.9	130.4	130.2	130.3	129.0	128.9	128.95	127.7	127.6	127.65
6	76.25	130.8	130.2	130.5	129.4	128.8	129.1	128.3	127.7	128.0	127.1	12618	126.95
7	84.50	128.9	129.2	129.05	128.0	128.1	128.05	127.1	127.2	127.15	126.3	126.4	126.35
8	92.75	128.1	128.0	128.05	127.3	127.1	127.2	126.6	126.4	126.5	126.0	125.8	125.9
9	101.00	127.2	127.1	127.15	126.5	126.6	126.55	126.0	126.0	126.0	125.5	125.4	125.45
10	109.25	126.3	126.3	126.3	125.8	126.0	125.9	125.5	125.4	125.45	125.1	125.0	125.05
11	117.50	125.7	125.6	125.65	125.4	125.2	125.3	125.1	125.0	125.05	124.7	124.7	124.7
12	125.75	125.1	125.1	125.1	125.0	125.0	125.0	124.7	124.7	124.7	124.4	124.5	124.45

TABLE 3.11 (CONTN'D)

Flow(lps)		4.56			3.82			3.36			2.52		
Piez.	Test #	5			6			7			8		
No.	r_d(cm)	A	B	ave	A	B	ave	A	B	ave	A	B	ave
1	35.00	131.9	131.8	131.85	129.8	129.8	129.8	128.4	128.4	128.4	126.5	126.2	126.35
2	43.25	130.0	129.8	129.9	128.4	128.0	128.2	127.3	127.1	127.2	125.9	125.6	125.75
3	51.50	128.8	128.4	128.6	127.5	127.1	127.35	126.6	126.2	126.4	125.1	125.1	125.1
4	59.75	127.5	127.5	127.5	126.5	126.5	126.5	126.3	125.8	126.05	125.1	124.9	125.0
5	68.00	126.8	126.7	126.75	126.0	125.9	125.95	125.5	125.4	125.45	124.8	124.6	124.7
6	76.25	126.5	126.1	126.3	125.6	125.5	125.55	125.2	125.0	125.1	124.6	124.4	124.5
7	84.50	125.8	125.8	125.8	125.2	125.2	125.2	124.8	124.8	124.8	124.2	124.4	124.3
8	92.75	125.4	125.2	125.3	125.0	124.8	124.9	124.6	124.4	124.5	124.1	124.1	124.1
9	101.00	125.0	125.0	125.0	124.8	124.6	124.7	124.3	124.3	124.3	124.0	124.0	124.0
10	109.25	124.7	124.6	124.65	124.4	124.4	124.4	124.1	124.1	124.1	123.9	123.8	123.85
11	117.50	124.4	124.4	124.4	124.2	124.2	124.2	124.0	124.0	124.0	123.8	123.7	123.75
12	125.75	124.2	124.3	124.25	124.1	124.1	124.1	123.9	132.9	132.9	123.7	123.6	123.65

TABLE 3.12 Converging Flow Data for 1.51 cm Spheres
Temperature 23 °C

Flow(lps)		10.39			9.54			8.92			7.62		
Piez. No.	Test #	1			2			3			4		
	r_c(cm)	A	B	ave	A	B	ave	A	B	ave	A	B	ave
1	125.75	124.4	124.2	124.3	124.6	124.4	124.5	124.8	124.6	124.7	125.1	124.9	125.0
2	117.5	123.1	123.0	123.05	123.5	123.3	123.4	123.9	123.8	123.85	124.3	124.3	124.3
3	109.75	121.6	121.7	121.65	122.0	122.2	122.1	122.7	122.9	122.8	123.3	123.4	123.35
4	101.00	120.4	120.3	120.35	121.0	121.0	121.0	121.8	121.8	121.8	122.6	122.5	122.55
5	92.75	118.4	118.7	118.55	119.2	119.6	119.4	120.4	120.6	120.5	121.4	121.5	121.45
6	84.50	116.7	116.6	116.65	117.9	117.6	117.75	119.1	118.9	119.0	120.4	120.2	120.3
7	76.25	113.3	114.3	113.8	115.3	115.8	115.55	117.0	117.3	117.15	118.8	119.0	118.9
8	68.00	111.1	111.7	111.4	113.0	113.5	113.25	114.9	115.3	115.1	117.3	117.5	117.4
9	59.75	107.4	107.4	107.4	110.0	109.7	109.85	112.2	112.0	112.1	115.2	115.0	115.1
10	51.50	102.4	102.4	102.4	105.4	105.5	105.45	108.2	108.2	108.2	112.1	112.1	112.1
11	43.25	97.4	95.7	96.55	101.3	99.6	100.5	104.4	103.2	103.8	109.3	108.3	108.8
12	35.00	88.0	88.1	88.05	93.2	93.2	93.2	97.2	97.4	97.3	104.0	104.0	104.0

TABLE 3.12 (CONTN'D)

Flow(lps)		6.97			6.34			5.75			5.13		
Piez. No.	Test # / r_c (cm)	5			6			7			8		
		A	B	ave	A	B	ave	A	B	ave	A	B	ave
1	125.75	125.3	125.2	125.25	125.4	125.2	125.3	125.6	125.6	125.6	125.7	125.6	125.65
2	117.50	124.6	124.5	124.55	124.9	124.7	124.8	125.2	125.1	125.15	125.4	125.3	125.35
3	109.25	123.8	123.8	123.8	124.2	124.2	124.2	124.7	124.7	124.7	125.0	125.0	125.0
4	101.00	123.1	123.1	123.1	123.6	123.6	123.6	124.3	124.2	124.25	124.6	124.6	124.6
5	92.75	122.1	122.2	122.15	122.7	122.7	122.7	123.6	123.6	123.6	124.1	124.0	124.05
6	84.50	121.2	121.0	121.1	122.0	121.8	121.9	213.0	122.8	122.9	123.6	123.3	123.45
7	76.25	119.8	119.9	119.85	120.8	120.8	120.8	122.0	122.0	122.0	122.6	122.7	122.65
8	68.00	118.5	118.6	118.55	119.6	119.8	119.7	121.0	121.1	121.05	121.9	122.0	121.95
9	59.75	116.8	116.5	116.65	118.3	118.0	118.15	119.0	119.6	119.3	120.9	120.7	120.8
10	51.50	114.2	114.1	114.15	116.0	116.0	116.0	118.0	118.0	118.0	119.4	119.3	119.35
11	43.25	111.7	110.8	111.25	114.0	113.2	113.6	116.2	115.6	115.9	118.0	117.5	117.75
12	35.00	107.2	107.1	107.15	110.2	110.0	110.1	112.9	113.1	113.0	115.4	115.3	115.35

TABLE 4.1 Range of Reynolds Number for the Parallel Flow Tests

	Minimum Reynolds No.	Maximum Reynolds No.
1.51 cm Spheres	960	4830
2.06 cm Rocks	1630	5950
3.16 cm Rocks	1870	11050

TABLE 4.2 Range of Reynolds Number for the Radial Flow Tests

	Minimum Reynolds No.	Maximum Reynolds No.
1.51 cm Spheres	450	5000
2.06 cm Rocks	475	5540
3.16 cm Rocks	680	7993
1.51 cm Spheres (converging)	720	5200

TABLE 4.3 Porosity and Wall Corrections for all the Tests

	Porosity Correction		Wall Correction	
	a	b	a	b
1.51 cm spheres	0.0105	0.0082	0.0151	0.0104
2.06 cm Rocks	0.0096	0.0104	0.0112	0.0122
3.16 cm Rocks	0.0060	0.0066	0.0064	0.0075
1.51 cm Spheres (converging)	0.0124	0.0089	0.0151	0.0104

TABLE 4.4 a and b Values for the Parallel and Radial Flow Tests

	a	b
Prallel Tests		
1.51 cm Spheres	0.0146	0.0097
2.06 cm Rocks	0.0107	0.0110
3.16 cm Rocks	0.0060	0.0066
Radial Tests		
1.51 cm Spheres	0.0108	0.0092
2.06 cm Rocks	0.0101	0.0120
3.16 cm Rocks	0.0064	0.0079
1.51 cm Spheres (converging)	0.0128	0.0076

TABLE 4.5 A Comparison of the a and b Values for all the Tests

	Parallel		Corrected		Radial		% Change of b
	a	b	a	b	a	b	
1.51 cm Spheres (diverging)	0.0146	0.0097	0.0108	0.0088	0.0108	0.0092	+4.5
1.51 cm Spheres (converging)	0.0146	0.0097	0.0128	0.0095	0.0128	0.0076	-22.0
2.06 cm Rocks (diverging)	0.0107	0.0110	0.0101	0.0114	0.0101	0.0120	+5.0
3.16 cm Rocks (diverging)	0.0060	0.0066	0.0064	0.0075	0.0064	0.0079	+5.3

APPENDIX C

REFERENCES

1. AHMED, N. and SUNADA, D.K., "Nonlinear Flow in Porous Media", J. of Hyd. Div., Proc. of ASCE, Vol. 95, No. HY6, Nov. 1969.

2. DUDGEON, C.R., "Wall Effects in Permeameters", J. of Hyd. Div., Proc. of ASCE, Vol. 93, No. HY5, Sept. 1967.

3. ESCANDE, L., "Experiments Concerning the Infiltration of Water Through Rockmass", Proc. of Minnesota International Hyd. Convention, 1953.

4. FORCHHEIMER, P.H., "Wasserbewegun Durch Boden", Zeitschrift Des Vereines Deutecher Ingenierre, No. 49, 1901.

5. GILL, M.A., "Analysis of Permeameter Data To Obtain Parameters of Non-Darcy Flow", J. of Hydrology, Vol. 32, 1977.

6. HARR, M.E., "Groundwater and Seepage", McGraw-Hill Book Company, New York, 1962.

7. IZBASH, S.V., "O Filtracii V Kropnozernstom Materiale", Izv. Nauchnoissled, Inst. Giprotechniki (N116), Leningrad, U.S.S.R., 1931.

8. KOVACKS, G., "Seepage Law for Microseepage", Proc. of X111 Congress IAHR, Vol. 4, Kyoto, Japan, Sept. 1969.

9. McCORQUODALE, J.A., HANNOURA, A.A., AND NASSER, M.S., "Hydraulic Conductivity in Rockfill", J. of Hydraulic Research, Vol. 16, No. 2, 1978.

10. McCORQUODALE, J.A., "Finite Element Analysis of Non-Darcy Flow", A Thesis Presented to the University of Windsor in Partial Fullfillment of the Requirements for The P.H.D. Degree in Civil Engineering, Windsor, Canada, 1970.

11. NASSER, M.S., "Radial Non-Darcy Flow Through Porous Media", A Thesis Presented to the University of Windsor in Partial Fullfillment of the Requirements of the M.A. Sc. Degree in Civil Engineering, Windsor, Canada, 1970.

12. NASSER, M.S., "Theoretical and Experimental Analysis of Wave Motion in Rockfill Structures", A Thesis Presented To The University of Windsor in Partial Fullfillment of The Requirements for The P.H.D. Degree in Civil Engineering, Windsor, Canada, 1974.

13. NEVILLE, A.M., KENNEDY, J.B., "Basic Statistical Methods for Engineers and Scientists", International Textbook Co., Scranton, Pa., 1964.

14. PEARSON, F.H., McDONNELL, A.J., "Characterization of Coarse Porous Media", J. of Envirn. Engr. Div., Proc. of ASCE, Vol. 103, No. EE4, Aug., 1977.

15. ROSE, H.E., "Fluid Flow Through Beds of Granular Media", Some Aspects of Fluid Flow, Edward Arnold and Co., London, England, 1951.

16. SCHEIDEGGER, A.E., "The Physics of Flow Through Porous Media", The MacMillan Co., New York, 1960.

17. SLEPICKA, F., "The Laws of Filtration and Limits of Their Validity", IAHR, 9th. Congress, Dubrounir, Yugoslavia, 1961.

18. SONI, J.P., ISLAM, N., BASAK, P., "An Experimental Evaluation of Non-Darcian Flow in Porous Media", J. of Hydrology, Vol. 38, 1978.

19. STREETER, V.L., WYLLE, E.B., "Fluid Mechanics", McGraw-Hill Book Co., Sixth Ed., 1975.

20. VRIES, J. DE, "Prediction of Non-Darcy Flow in Porous Media", J. of IRR. and Drain D.W., Vol. 105, No. IR2, June, 1979.

21. WARD, J.C., "Discussion of Resistance To Laminar Flow Through Porous Media", J. of Hyd. Div., Proc. of ASCE, Vol. 93, No. HY2, March 1917.

22. WARD, J.C., "Turbulent Flow in Porous Media", J. of Hyd. Div., Proc. of ASCE, Vol. 90, No. HY5, Sept. 1964.

23. WRIGHT, D.E., "Nonlinear Flow Through Granular Media", J. of Hyd. Div., Proc. of ASCE, Vol. 94, No. HY4, July, 1968.

APPENDIX D

NOMENCLATURE

NOMENCLATURE

A	Permeameter X-Sectional Area
a	Laminar Coefficient of the Forchheimer Equation
a'	Laminar Coefficient Corrected for Porosity
a''	Laminar Coefficient Corrected for Wall Effects
a_c	Corrected Laminar Coefficient for Converging Flow
a_d	Corrected Laminar Coefficient for Diverging Flow
a_p	Corrected Laminar Coefficient for Parallel Flow
B	Resistance Coefficient
b	Turbulent Coefficient of the Forchheimer Equation
b'	Turbulent Coefficient Corrected for Porosity
b''	Turbulent Coefficient Corrected for Wall Effects
b_c	Corrected Turbulent Coeffieint for Converging Flow
b_d	Corrected Turbulent Coefficient for Diverging Flow
b_p	Corrected Turbulent Coefficient Parallel Flow
C	Resistance Coefficient
C_m	Correction for Porosity
C_w	Correction for Wall Effects
D_m	Mean Nominal Diameter
d_e	Equivalent Diameter
d_n	Nominal Particle Diameter
d_r	Pore Hydraulic Radius
d_r'	Effective Pore Hydraulic Radius
f	Resistance Coefficient

f_e	Friction Factor
f_0	Friction Factor
G	Particle (Shape, Size and Roughness) Coefficient
g	Acceleration Due to Gravity
i	Hydraulic Radius
k	Permeability or Hydraulic Conductivity
L_e	Effective Perimeter
L_t	Total Perimeter
M	Resistance Coefficient
m	Porosity
m_p	Porosity in Parallel Permeameter
m_r	Porosity in Radial Permeameter
n	Resistance Equation Exponent
Q	Flow
q	Microscopic Velocity
R	Reynolds Number
R_p	Pore Reynolds Number
R_w	Wright Reynolds Number
r_c	Radius of Convergence
r_d	Radius of Divergence
S_a	Surface Area of Particle
S_s	Specific Surface of Particle
T	Tortuosity
V_m	Volume of Particle
V_t	Total Volume

V_v	Volume of Voids
v	Macroscopic Velocity
W_m	Weight of Particle
w	Width of Permeameter
X	X-Sectional Constant (1.8 for Circular and 2.0 for Rectangular Permeameters)

GREEK LETTERS

α	Resistance Coefficient
β	Resistance Coefficient
γ_m	Specific Weight of Porous Media
θ	Angle of Divergence/Convergence
λ	Shape Factor
μ	Dynamic Viscosity
ν	Kinematic Viscosity
ξ	Resistance Coefficient
ρ	Density
σ_g	Standard Deviation of Mean Nominal Diameter
ϕ	Piezometric Head
ψ	Resistance Coefficient
ϕ	Resistance Coefficient